Supplementary information for *Isoform switching facilitates period control in the Neurospora crassa circadian clock.*, O.E. Akman et al.

Contents

1 Introduction **2**

2 The *Neurospora* models used **2**

2.1 Model 1 . . . 2

2.2 Model 2 . . . 3

3 Finding starting solutions of the models **4**

3.1 Model 1 . . . 4

3.2 Model 2 . . . 5

4 Isoform switching as a mechanism for global temperature compensation and period control **6**

4.1 Incorporating temperature in the models . . . 6

4.2 Local and global compensation . . . 7

4.3 Isoform switching . . . 8

4.4 Direct compensation of the models . . . 9

4.5 Results . . . 10

4.5.1 Wild-type simulations obtained using isoform switching . . . 10

4.5.2 Comparison with single-point compensation . . . 11

5 Simulating compensation mutants producing only one form of FRQ **12**

5.1 Modelling of strains producing mainly s-FRQ . . . 12

5.2 Modelling of strains producing mainly l-FRQ . . . 12

5.3 Results . . . 12

6 Quantifying the relationship between FRQ level and rhythmicity **14**

6.1 Verification of an increasing lower threshold for rhythmicity . . . 15

6.2 Prediction of an upper threshold for rhythmicity . . . 15

7 Variation of entrainment phase with temperature **16**

8 Robustness of the isoform switching mechanism **16**
8.1 Switching through simulated annealing 16
8.2 Results 17

9 Simulating compensation mutants resulting from changes in FRQ stability **18**
9.1 The form of the overall FRQ loss rate in models 1 and 2 18
9.2 Modelling the mutants by varying the loss rate 18

References **19**

Figures **22**

Tables **29**

1 Introduction

This document provides detailed descriptions of the *Neurospora* models used in the main paper, together with the mathematical background for the discussions of period control and rhythmicity therein.

2 The *Neurospora* models used

Two models of the *Neurospora* circadian clock were used to illustrate how the parallel, temperature-dependent FRQ feedback loops can give rise to temperature compensation and period control through isoform switching. The first of the models - referred to here as model 1 - is an extension of an existing model involving only the *frq* gene; it is included to demonstrate that the isoform switching mechanism is not specific to a particular set of equations. The second is a more realistic model incorporating the *wc-1* gene in addition to *frq*. This is the model discussed in the main paper, and will referred to in what follows as model 2. SBML versions of both models are available from the *Molecular Systems Biology* website (www.nature.com/msb). These were tested using the Systems Biology Workbench simulation tool (http://www.sys-bio.org/research/sbwIntro.htm). Matlab versions of the models together with the parameter sets used for all simulations presented in this work are available by request from oakman@staffmail.ed.ac.uk.

2.1 Model 1

Model 1 was obtained by modifying that of Leloup et al ([17]) to incorporate the two FRQ forms:

$$\dot{M}_F = (v_s + \theta(t)) \frac{K_I^n}{K_I^n + (F_N + F'_N)^n} - v_m \frac{M_F}{K_m + M_F} \quad (1)$$

$$\dot{F}_C = k_s M_F - v_d F_C - k_1 F_C + k_2 F_N \quad (2)$$

$$\dot{F}_N = k_1 F_C - k_2 F_N \quad (3)$$

$$\dot{F}'_C = k'_s M_F - v'_d F'_C - k'_1 F'_C + k'_2 F'_N \quad (4)$$

$$\dot{F}'_N = k'_1 F'_C - k'_2 F'_N. \quad (5)$$

Here, M_F represents the concentration of *frq* mRNA, while F_C and F_N are the concentrations of s-FRQ in the cytoplasm and nucleus respectively. The quantities F'_C and F'_N denote the equivalent

quantities for l-FRQ. The effect of light is represented by the forcing term $\theta(t)$, which acts by increasing the transcription rate of *frq*. $\theta(t)$ switches rapidly between 0 and a maximum value of 1 at lights-on, switching back to 0 at lights-off.

Equations (1)-(5) can be considered as a minimal model of the *Neurospora* clock, incorporating only a simplified version of the core negative feedback loop in which FRQ directly represses *frq* transcription. It should be noted from (1) that it is assumed the two FRQ forms are equally effective as repressors of *frq*.

2.2 Model 2

The network diagram corresponding to model 2 is shown in figure 1 of the main paper. The model equations are

$$\dot{M}_F = a_1 \frac{\left(P_W^L\right)^n}{\left(1+\frac{P_F+P_F'}{b_1}\right)\left(\left(P_W^L\right)^n + b_2^n\right)} + a_2 \frac{\left(P_W\right)^m}{\left(1+\frac{P_F+P_F'}{b_3}\right)\left(\left(P_W\right)^m + b_4^m\right)} - d_1 \frac{M_F}{M_F+b_5} \tag{6}$$

$$\dot{P}_F = a_3 \int_{-\infty}^{t} M_F(s)\, g_{f_1}(t-s)\, e^{-\gamma_1(t-s)} ds - d_2 P_F \tag{7}$$

$$\dot{P}_F' = a_3' \int_{-\infty}^{t} M_F(s)\, g_{f_1'}(t-s)\, e^{-\gamma_1'(t-s)} ds - d_2' P_F' \tag{8}$$

$$\dot{M}_W = a_4 + a_5 \frac{\left(P_W^L\right)^k}{\left(P_W^L\right)^k + b_6^k} - d_3 \frac{M_W}{M_W+b_7} \tag{9}$$

$$\dot{P}_W = \int_{-\infty}^{t} M_W(s)\left(a_6 + a_7\left(P_F(s)+P_F'(s)\right)\right) g_{f_2}(t-s)\, e^{-\gamma_2(t-s)} ds - d_4 \frac{P_W}{P_W+b_8} - r_1\theta(t) P_W + r_2 P_W^L \tag{10}$$

$$\dot{P}_W^L = r_1\theta(t) P_W - r_2 P_W^L - d_5 \frac{P_W^L}{P_W^L+b_9}. \tag{11}$$

Here, the variables M_F and M_W denote the concentrations of *frq* and *wc-1* mRNA respectively. P_W^L is the concentration of light-activated WC-1, in which light has induced the binding of a flavin chromophore (FAD) to the LOV-sensing domain of the protein. P_W represents the concentration of the non light-activated protein. The levels of the two FRQ forms are represented by the variables P_F (s-FRQ) and P_F' (l-FRQ).

Equations (6)-(11) are a more comprehensive model of the *Neurospora* circuitry than (1)-(5). The role of *wc-1* in the negative feedback loop is incorporated, with the repressive action of FRQ on *frq*-bound WC-1 modelled as a noncompetitive inhibition process (see equation (6)). The model also includes the positive feedback loop in which FRQ enhances the production of WC-1 (see equation (10)). As for model 1, the effect of light is represented by a term $\theta(t)$ that increases from 0 to a maximum value of 1 at lights-on. This causes a rapid increase in the forward rate of the reaction $P_W \rightleftharpoons P_W^L$, modelling the rise in the relative concentration of FAD-bound WC-1 observed with increasing light levels [9]. The sudden switch to the light-activated WC-1 form results in enhanced transcription of *frq* through the first term of equation (6); additionally, it raises the transcription rate of *wc-1* through the second term of (9), reflecting the loss of *wc-1* light-responses in *wc-1* mutant backgrounds [18].

A relative novelty of the model is the way in which the protein pathways have been represented. Many mathematical models of circadian networks employ sequences of protein modifications (usually phosphorylation and nuclear transport) in order to produce the delays necessary for self-sustained oscillations to be generated [15]. An alternative method has been used in the construction of (6)-(11). In equations (7), (8) and (10), the distribution of times required for a FRQ or WC-1 protein to be modified and transported to become a transcription factor (TF) is assumed to be an Erlang function with scale parameter equal to f_i and shape parameter equal to 2:

$$g_{f_i}(t) = f_i^2 t e^{-f_i t}. \tag{12}$$

This distribution has mean delay $\frac{2}{f_i}$ - representing the average delay between the translation of a protein and its conversion into transcription factor - and variance $\frac{2}{f_i^2}$ - representing the mean deviation from the average. The term $e^{-\gamma_i t}$ that post-multiplies the Erlang term corresponds to the loss of proteins during modification, with γ_i quantifying the rate of this loss [23]. An advantage of this approach is that there is a reduction in the effective number of model parameters; also, no *a priori* assumptions have to be made regarding the processes underlying the oscillation-generating delays. The equations were solved by writing the integrodifferential equations (7), (8) and (10) as equivalent chains of linear ordinary differential equations [23].[1]

Finally, it should be noted that as in model 1, s-FRQ and l-FRQ are assumed to be equally effective in repressing *frq* transcription (see equation (6)). In addition, they are also assumed to be equally effective in enhancing the rate of WC-1 production (see equation (10)).

3 Finding starting solutions of the models

In order to implement global temperature compensation and period tuning through isoform switching, solutions of the two models representative of the relevant experimental data on *Neurospora* rhythms were first obtained. The free-running period of *Neurospora* is approximately 22h [1]. In constant darkness, *frq* mRNA is at a minimum level early in the subjective night, peaking after about 12h circadian time (CT). FRQ peaks 4-6h after its transcript, reaching minimum levels approximately 12h later. *wc-1* mRNA is expressed constitutively, with its protein product oscillating roughly in antiphase with FRQ [16], [25], [6], [9], [10]. In constant light, levels of both *frq* mRNA and FRQ are elevated and arrhythmic, indicating that the circadian clock is not functioning [5], [3]. Dark-to-light transfers induce rapid increases in both *frq* and *wc-1* mRNA levels, while light-to-dark transfers cause rapid decreases in the level of *frq* [5], [33]. These light-induced changes in mRNA levels provide the molecular basis for the entrainment of the clock by light-dark (LD) cycles [19].

3.1 Model 1

The first step in finding a suitable starting parameter set for model 1 was to set all primed parameters (representing translation, degradation and transport of l-FRQ species) equal to their unprimed counterparts (representing the equivalent processes for s-FRQ). This enabled (1)-(5) to be reduced to a 3-dimensional model involving only the total amounts of cytoplasmic and nuclear proteins, $(F_C + F'_C)$ and $(F_N + F'_N)$ respectively. Next, 250000 randomly distributed points were generated

[1] Within this framework, the variables in the chains can be considered as intermediate protein species (e.g. cytoplasmic proteins in different phosphorylation states).

in the resulting 9-dimensional parameter space. The points were chosen so that all parameters were bounded between 0 and 10, with the exception of the Hill coefficient n, which was bounded between 4 and 8.[2] For each point, the equations were integrated for 600h in simulated DD conditions to remove transients. The equations were then integrated for a further 600h, and the times of repeated intersections with a Poincaré section used to assess whether the solution was likely to be periodic. Candidate periodic solutions identified in this manner were used as the seed of a boundary value solver to check for true periodicity [32]. The parameter sets generating periodic solutions were then rescaled so as to give a period of 22h. For each of these sets, the technique used to check for periodicity in DD was repeated for simulated 12:12 LD cycles, leading to solutions with the correct free-running period that could be entrained by light over a range of 24h photoperiods.

The solutions of the reduced model obtained in this way were then converted into solutions of the full 5-d model by setting the values of each primed/unprimed parameter pair equal to that of the corresponding parameter in the reduced model, with the exception of the FRQ translation rates k_s and k'_s, which were set to half the translation rate in the reduced model. This gave symmetric solutions of (1)-(5) with $F_C = F'_C$ and $F_N = F'_N$. Next, the symmetry of the solutions was broken by randomly perturbing the l-FRQ loop parameters $\{k'_s, v'_d, k'_1, k'_2\}$. Symmetry-broken parameter sets with $k_s > k'_s$ generating oscillatory solutions where the level of s-FRQ was greater than that of l-FRQ at the phase of maximal FRQ expression were rescaled to give 23h periods, and then checked for entrainment to 12:12 LD cycles as described above. These parameter sets were used as the starting points for isoform switching at the lower end of the temperature range.

3.2 Model 2

In order to find starting parameter sets for model 2, a parameter selection technique based on the construction of a qualitative cost function was employed [21], [22]. As for model 1, all primed parameters of (6)-(11) were first set equal to their unprimed counterparts. This enabled the system to be reduced to a 5-dimensional model involving only the total amount of FRQ transcription factor, $P_F + P'_F$. 1 million Sobol quasi-random points were then chosen in the resulting 30-dimensional parameter space, as described in [21]. These points were chosen so that all parameters were bounded between 0 and 10, excluding n, m, k, f_1, f_2, γ_1 and γ_2. The Hill coefficients n, m and k were bounded between 1 and 4 to exclude solutions with unrealistically high levels of transcription factor/promoter cooperativity. The scale parameters f_1 and f_2 of the Erlang distributions were bounded between $\frac{2}{15}$ and $\frac{10}{15}$ in order to bound the initial mean delays in the modification of translated FRQ/WC-1 into transcription factor between 3h and 15h. Finally, γ_1 and γ_2 were bounded between 0 and 0.2 in order to exclude solutions in which intermediate protein species had unrealistically low survival rates.

Following [21] and [22], each Sobol point was assigned a cost function score $C(k_i)$, composed of a sum of squared terms. The principal terms in $C(k_i)$ were chosen to ensure that: 1) the solution oscillated with a period close to 22h in DD cycles; 2) the phases of the solution in DD were close to those observed experimentally; and 3) the solution was entrained to 12:12 LD cycles. The 50 solutions with the lowest cost function scores were then optimised using a variant of the simulated annealing algorithm described in [13]. At each step of the algorithm, the k_is were

[2] Although it is possible to obtain oscillatory solutions for equations (1)-(5) with Hill coefficients as small as 1 ([12]), n was set greater than 4 in order to generate a greater number of parameter sets to use as starting points for the optimisation procedure.

randomly perturbed yielding a new cost value C'. The perturbation was accepted with probability $\min\left\{e^{\left(-(C'-C)/A_T\right)}, 1\right\}$, where A_T is a parameter (the annealing temperature) that decreases linearly with step number to 0. Perturbations decreasing C were therefore always accepted while perturbations increasing C were less frequently accepted, with the probability of acceptance decreasing with time. This gave rise to a hill-climbing optimisation algorithm able to locate multiple minima of C [13], [21]. During the annealing process, Hill coefficients were kept bounded between 1 and 4 while all other parameters were allowed to vary freely. For each of the 50 low cost solutions, 100000 annealing steps were used with the starting annealing temperature set equal to the greatest initial cost value.

Following the method for model 1, the optimised solutions of the reduced 5-d model were converted into solutions of the full model (6)-(11) by setting the values of each primed/unprimed parameter pair equal to that of the corresponding parameter in the 5-d model, with the exception of the FRQ translation rates a_3 and a_3' which were set to half the translation rate in the reduced model. This yielded symmetric solutions of (6)-(11) with $P_F = P_F'$. As for model 1, asymmetric solutions were obtained through random perturbations of the l-FRQ loop parameters, $\{a_3', f_1', \gamma_1', d_2'\}$. Those parameter sets with $a_3 > a_3'$ yielding periodic solutions with levels of s-FRQ greater than l-FRQ at the phase of maximal FRQ expression were rescaled to give a period of 23h and checked for entrainment to 12:12 LD cycles. These parameter sets were used as the starting points for isoform switching at the lower end of the temperature range.

4 Isoform switching as a mechanism for global temperature compensation and period control

4.1 Incorporating temperature in the models

Following the approach of Ruoff ([30], [29], [31]) the temperature dependence of a given parameter k_j of the *Neurospora* models was assumed to be described by the Arrhenius equation:

$$k_j = A_j e^{-\frac{E_j}{RT}}. \tag{13}$$

Here, A_j and E_j are respectively the collision factor and activation energy of the process associated with k_j, R is the universal gas constant (8.3145 x 10^{-3} kJ mol^{-1} K^{-1}) and T is temperature. Exceptions to this were Hill coefficients (n in model 1, n, m and k in model 2) and the s- and l-FRQ translation rates r_S and r_L ($r_S = k_s, r_L = k_s'$ for model 1; $r_S = a_3, r_L = a_3'$ for model 2). Hill coefficients were assumed to be independent of temperature, while the temperature dependence of r_S and r_L was modelled by the sigmoidal functions

$$r_S(T) = a_1 \tanh\left(b_1\left(T - T_{S_1}\right)\right) + c_1, \tag{14}$$

$$r_L(T) = a_2 \tanh\left(b_2\left(T - T_{S_2}\right)\right) + c_2. \tag{15}$$

The function $a_i \tanh\left(b_i\left(T - T_{S_i}\right)\right) + c_i$ varies smoothly between the values $c_i + a_i$ and $c_i - a_i$ as T is varied, crossing c_i at the switching temperature $T = T_{S_i}$ with a slope determined by the value of b_i. By choosing a_i, b_i and c_i in (14) and (15) appropriately, translation profiles could be obtained modelling the experimentally observed shift with increasing temperature of the preferred translation initiation site on the *frq* ORF from AUG #3 (the initiation codon of s-FRQ) to AUG #1 (the initiation codon of l-FRQ) [20], [4], [8].

4.2 Local and global compensation

For a given clock model, the period p can be written as $p = p(T) = p(k_1(T), \ldots, k_m(T))$ where T acts through the model parameters $\{k_1, \ldots, k_m\}$. Taylor expanding the period about a particular temperature T_0 gives the expression below:

$$p(T) = p(T_0) + \frac{dp}{dT}(T_0)(T - T_0) + \frac{d^2p}{dT^2}(T_0)(T - T_0)^2 + O\left(|T - T_0|^3\right). \tag{16}$$

Applying the chain rule leads to the following equations for $\frac{dp}{dT}$ and $\frac{d^2p}{dT^2}$ involving the k_js:

$$\frac{dp}{dT} = \sum_{j=1}^{m} \frac{\partial p}{\partial k_j}\frac{dk_j}{dT}, \tag{17}$$

$$\frac{d^2p}{dT^2} = \sum_{j=1}^{m} \frac{\partial p}{\partial k_j}\frac{d^2k_j}{dT^2} + \sum_{i,j=1}^{m} \frac{\partial^2 p}{\partial k_i \partial k_j}\frac{dk_i}{dT}\frac{dk_j}{dT}. \tag{18}$$

Equation (16) shows that for T sufficiently close to T_0,

$$p(T) \approx p(T_0) + \frac{dp}{dT}(T_0)(T - T_0).$$

Consequently, if $\frac{dp}{dT}(T_0) = 0$, the period of the clock will be roughly invariant in an interval containing T_0; the system will therefore be locally compensated at this point. Labelling the k_js so that $k_{m-1} = r_S$ and $k_m = r_L$, it follows from (13) that for the *Neurospora* models considered here, $\frac{dp}{dT}$ can be written as shown below:

$$\frac{dp}{dT} = \frac{1}{RT^2}\sum_{j=1}^{m-2} \frac{\partial p}{\partial k_j}k_j E_j + \frac{\partial p}{\partial r_S}r'_S + \frac{\partial p}{\partial r_L}r'_L. \tag{19}$$

This expression can also be written as

$$\frac{dp}{dT} = p\left(\frac{1}{RT^2}\sum_{j=1}^{m-2} C_j^p E_j + C_{m-1}^p \frac{r'_S}{r_S} + C_m^p \frac{r'_L}{r_L}\right), \tag{20}$$

where $C_j^p = \frac{\partial \log(p)}{\partial \log(k_j)}$ is the control coefficient or elasticity associated with k_j [30], [14] (cf. equation (1) of the main paper). For both models, the k_js can be subdivided into 3 functional groups: the parameters associated with the s-FRQ loop L_S, those associated with the l-FRQ loop L_L, and the remaining parameters N. The condition $\frac{dp}{dT} = 0$ for local temperature compensation at T_0 can therefore be expressed in the form:

$$\frac{1}{RT^2}\left(\sum_{j\in L_S\setminus r_S} \frac{\partial p}{\partial k_j}k_j E_j + \sum_{j\in L_L\setminus r_L} \frac{\partial p}{\partial k_j}k_j E_j + \sum_{j\in N} \frac{\partial p}{\partial k_j}k_j E_j\right) + \frac{\partial p}{\partial r_S}r'_S + \frac{\partial p}{\partial r_L}r'_L = 0. \tag{21}$$

Global temperature compensation - that is obtaining a system with a relatively invariant period over a significant range of temperatures $T_1 < T < T_2$, can then be interpreted as the process of tuning the terms of the balance equation (21) so that it is approximately satisfied over the whole range (T_1, T_2). One way this could be achieved is by finding a set of parameters that simultaneously solve the balance equation at a number of intermediate temperatures in (T_1, T_2); for a significant range this will require the independent adjustment of a large number of parameters. In principal, compensation could also be attained over (T_1, T_2) through a single local compensation

at an intermediate temperature [29], [30] (this mechanism will be referred to here as single-point compensation). Setting $\frac{dp}{dT} = 0$ in (16) and substituting (13) into (18) implies the period of a system compensated at T_0 is locally of the form,

$$p\left(T\right) \approx p\left(T_0\right) + \frac{d^2p}{dT^2}\left(T_0\right)\left(T - T_0\right)^2, \tag{22}$$

where[3]

$$\begin{aligned}\frac{d^2p}{dT^2} &= \frac{1}{RT^2}\sum_{j=1}^{m-2}\left(\frac{1}{RT^2}\frac{\partial p}{\partial k_j}k_jE_j^2 + 2\left(\frac{\partial^2 p}{\partial k_j \partial r_S}r'_S + \frac{\partial^2 p}{\partial k_j \partial r_L}r'_L\right)k_jE_j\right) \\ &\quad + \frac{1}{\left(RT^2\right)^2}\sum_{i,j=1}^{m-2}\frac{\partial^2 p}{\partial k_i \partial k_j}k_ik_jE_iE_j + \frac{\partial p}{\partial r_S}r''_S + \frac{\partial p}{\partial r_L}r''_L + \frac{\partial^2 p}{\partial r_S^2}\left(r'_S\right)^2 + \frac{\partial^2 p}{\partial r_L^2}\left(r'_L\right)^2 \\ &\quad + 2\left(\frac{1}{T}\left(\frac{\partial p}{\partial r_S}r'_S + \frac{\partial p}{\partial r_L}r'_L\right) + \frac{\partial^2 p}{\partial r_S \partial r_L}r'_Sr'_L\right).\end{aligned} \tag{23}$$

(22) suggests that if $\frac{d^2p}{dT^2}\left(T_0\right)$ is sufficiently small, $p\left(T\right)$ will be relatively invariant over (T_1, T_2), yielding a globally compensated system. However, as can be seen in (23), unless the scaled first and second derivatives of period with respect to parameter, $k_i\frac{\partial p}{\partial k_i}$ and $k_ik_j\frac{\partial^2 p}{\partial k_i \partial k_j}$, are small at T_0, tuning of the system to obtain $\frac{d^2p}{dT^2}$ close to 0 will again involve the adjustment of a large number of independent parameters. In the general case, one would expect a number of these derivatives to be of significant magnitude: indeed, for both models considered here, a large proportion of the scaled period derivatives are of order 1 or more (see tables 1 and 6 and figure 1). It follows, using typical values for the E_js, that $\frac{d^2p}{dT^2}\left(T_0\right)$ can be of order 0.1 or more. Hence, for realistic models, a significant quadratic variation of period should be observed in a system obtained through single-point compensation.

4.3 Isoform switching

Isoform switching is an alternative approach to global compensation which requires the adjustment of only 3 parameters (i.e. it is a codimension 3 process). Two of these parameters tune the system to satisfy the balance equation (21) at T_1 and T_2, giving local compensation at the upper and lower ends of the temperature range. The third parameter adjusts the difference $\Delta p = p(T_2) - p(T_1)$ between the periods at the temperature extremes to be close to 0, yielding a globally compensated system. The change in the relative abundance of the FRQ forms with temperature ([20], [8]) means that these adjustments can effectively be made independently of each other; this is in contrast to the compensation mechanisms discussed in section 4.2, in particular single-point compensation.

The derivation of globally compensated solutions of the *Neurospora* models through direct application of isoform switching is described below. Section 8 demonstrates how such systems could arise through stochastic parameter changes that mimic evolutionary processes. In all simulations shown here, T_1 and T_2 were set equal to 18°C and 30°C respectively, in accordance with the physiological range considered in [20].

[3] $p\left(T_0\right)$ and $\frac{d^2p}{dT^2}\left(T_0\right)$ are referred to as a and b respectively in the main paper.

4.4 Direct compensation of the models

Step 1. Balancing using the s-FRQ loop at T_1

For both models, the starting point for the compensation at T_1 was taken to be a parameter set yielding a 23h period cycle with $r_S(T_1) > r_L(T_1)$, such that the level of s-FRQ was greater than that of l-FRQ at the phase of maximal FRQ expression. These solutions reflect the oscillation periods and relative FRQ levels observed experimentally at the lower end of the physiological range in the *frq* wild-type (WT) construct KAJ120 in the experiments of Liu et al. [20]; their derivation was described in section 3. Since $r_S(T_1) > r_L(T_1)$, the terms for the s-FRQ loop dominate those for the l-FRQ loop in (21), allowing the condition for local compensation at T_1 to be approximated by:

$$\frac{1}{RT_1^2}\left(\sum_{j\in L_S\setminus r_S}\frac{\partial p}{\partial k_j}k_jE_j+\sum_{j\in N}\frac{\partial p}{\partial k_j}k_jE_j\right)+\frac{\partial p}{\partial r_S}r_S'=0.$$

Substituting (14) into the above and rearranging leads to the following balance equation:

$$\sum_{j\in L_S\setminus r_S}\frac{\partial p}{\partial k_j}k_jE_j+\sum_{j\in N}\frac{\partial p}{\partial k_j}k_jE_j=-RT_1^2a_1b_1\mathrm{sech}^2\left(b_1\left(T_1-T_{S_1}\right)\right)\frac{\partial p}{\partial r_S}. \tag{24}$$

Specification of the crossover temperature T_{S_1}, the crossover slope b_1 and the value of the s-FRQ translation rate r_S at T_2 determines the values of a_1 and c_1 (cf. (14)). For both models, T_{S_1} was set close to the midpoint of (T_1, T_2), b_1 was chosen to lie between 0 and 0.5 and $r_S(T_2)$ was set equal to $\alpha r_S(T_1)$ for some $0.8 \leq \alpha \leq 1$. The derivatives $\frac{\partial p}{\partial k_j}$ and $\frac{\partial p}{\partial r_S}$ can be calculated from analytical expressions obtained using limit cycle perturbation theory, as described in [27]. Following the computation of these derivatives, all terms in (24) are determined, with the exception of the activation energies E_j. To balance using the s-FRQ loop, it is therefore only necessary to find a set of E_js solving the resulting linear equation. This can be done by extending (24) into a consistent system of linear equations.

Step 2. Obtaining the correct period at T_2

Following the calculation of the activation energies E_j needed to balance using the s-FRQ loop at T_1, the corresponding collision factors A_j were calculated from (13), enabling the values of the parameters in the L_S and N groups to be determined at the upper temperature T_2. Setting the L_L parameters equal to their values at T_1 and setting $r_L(T_2)$ equal to $r_S(T_1)$ yielded a putative periodic solution of the model at $T = T_2$. If this solution was indeed periodic, its period was steered to the value 21h reported at the upper end of the physiological range in [20] by iteratively increasing the value of $r_L(T_2)$. This gave a solution with $r_L(T_2) > r_S(T_2)$, reflecting the greater translation of l-FRQ relative to that of s-FRQ at higher temperatures implied by experimental data [20], [8].

Step 3. Balancing using the l-FRQ loop at T_2

Since - by construction - r_L is greater than r_S at T_2, at this temperature the terms for the l-FRQ loop dominate those for the s-FRQ loop in (21), allowing the condition for local compensation at T_2 to be approximated by:

$$\frac{1}{RT_2^2}\left(\sum_{j\in L_L\setminus r_L}\frac{\partial p}{\partial k_j}k_jE_j+\sum_{j\in N}\frac{\partial p}{\partial k_j}k_jE_j\right)+\frac{\partial p}{\partial r_L}r_L'=0.$$

Substituting (15) into the above and rearranging leads to the following balance equation:

$$\sum_{j\in L_L\setminus r_L}\frac{\partial p}{\partial k_j}k_jE_j=-\sum_{j\in N}\frac{\partial p}{\partial k_j}k_jE_j-RT_2^2a_2b_2\mathrm{sech}^2\left(b_2\left(T_2-T_{S_2}\right)\right)\frac{\partial p}{\partial r_L}. \tag{25}$$

Specifying the crossover temperature T_{S_2} and the crossover slope b_2 determines the values of a_2 and c_2 (cf. (15)). As in Step 1, T_{S_2} was set close to the midpoint of (T_1, T_2), while b_2 was chosen to lie between 0 and 0.5. The derivatives $\frac{\partial p}{\partial k_j}$ and $\frac{\partial p}{\partial r_L}$ can again be calculated using the technique of [27], meaning that all terms in (25) are determined with the exception of the activation energies E_j on the left hand side. To balance using the l-FRQ loop, it is thus only required to find a set of these E_js solving the resulting linear equation.

Following the completion of step 3, the collision factors A_j corresponding to the E_js solving (25) can be calculated from (13); all temperature-dependent parameters are now determined across the full range (T_1, T_2). This gives a system which is locally compensated at both ends of the temperature range, that is with a relatively invariant period p in intervals around T_1 and T_2. Provided these intervals extend towards the central part of the range, p will then be relatively invariant across all of (T_1, T_2), giving a globally compensated clock.

4.5 Results

4.5.1 Wild-type simulations obtained using isoform switching

The upper panel of figure 2 shows the s- and l-FRQ translation-temperature profiles for a WT solution of the first *Neurospora* model (1)-(5) obtained through the direct application of isoform switching. Figure 2 of the main paper shows the corresponding profiles for a WT solution of the second *Neurospora* model (6)-(11) generated using the same method. The resulting variations in the levels of s-FRQ and l-FRQ with temperature are plotted in figure 3 below. For both models, an increase in the total amount of FRQ with temperature is accompanied by an increase in the l-FRQ:s-FRQ ratio, in agreement with experimental data [20], [8].

The period-temperature relationship for the WT solution of model 1 can be seen in figure 4 below, while that for model 2 is shown in figure 3 of the main paper. For both models, the variation in period is similar to that observed experimentally in [20], decreasing monotonically through 23h at the midpoint $T_C = \frac{1}{2}(T_1 + T_2)$ of the temperature range (T_1, T_2), with an overall decrease in period of roughly 2h. Time series of the solutions at the midpoint temperature T_C can be seen in figures 5 and 6. The parameter values, activation energies and period derivatives at the ends of the temperature range (T_1, T_2) are listed in tables 1 and 6, while the tanh function parameter values used to model the s-FRQ and l-FRQ translation-temperature profiles are given in tables 4 and 9. Finally, the parameters of the models for which the corresponding control coefficients are largest - and which thus contribute most to the change of period with temperature through (20) - are listed in tables 2 and 7. In addition to the FRQ translation rates $\{k_s, k_s'\}$ / $\{a_3, a_3'\}$, the dominant parameters can be identified as those determining the following:

1. The maximum transcription rate of *frq* mRNA (v_s/a_2).
2. The strength of repression of *frq* transcription by FRQ protein (K_I/b_3).
3. The maximum rate of *frq* degradation (v_m/d_1).

4. The rate of conversion of FRQ protein into transcription factor in the s-FRQ and l-FRQ loops ($\{k_1, k_1'\}$ / $\{f_1, f_1'\}$), and (for model 2) the degradation rate of the intermediate FRQ forms (γ_1, γ_1').

The effect on the period Q_{10} of perturbations to these parameters is shown in tables 3 and 8. Perturbations to parameters with Arrhenius dependence on temperature were obtained by changing the corresponding activation energy E_j so that the value of k_j at the midpoint temperature T_C was equal to the appropriate fraction of its original value. Perturbations to the translation parameters were obtained by uniformly scaling the translation profiles $r_S(T)$ and $r_L(T)$. It can be seen that for both models, the largest effect on the Q_{10}s are perturbations to the parameters determining the rates of FRQ translation and FRQ transcription factor conversion. Moreover, the simulations predict that perturbing these parameters in the s-FRQ loop will have a different effect to perturbing them in the l-FRQ loop. Indeed, while decreasing these rates in both loops yields a larger period compared to the WT - consistent with the negative control coefficients - reductions in the s-FRQ TF conversion rate increase the Q_{10} while decreases in the l-FRQ rate result in a reduced Q_{10}. In particular, the simulations for model 2 predict that perturbations to the system resulting in reduced l-FRQ translation rates, or a greater mean delay in the l-FRQ transcription-translation negative feedback loop, can lead yield an increasing period profile ($Q_{10} < 1$).

4.5.2 Comparison with single-point compensation

Figure 5 of the main paper (left panel) compares the period-temperature profile of the WT solution of model 2 obtained through isoform switching with one generated by locally compensating the corresponding symmetric starting parameter set (cf. section 3) at the midpoint T_C of the temperature range (T_1, T_2). After rescaling parameters to produce a cycle with period equal to the average of the simulated wild-type over (T_1, T_2), the symmetric system was locally compensated at T_C by finding energies satisfying (21), using the same computational methods as those employed to balance the asymmetric system at T_1 and T_2 in section 4.4.

It can be seen that although the locally compensated solution has a relatively invariant period in an interval containing T_C - with the quadratic behaviour predicted in section 4.2 - the system becomes arrhythmic as T_1 and T_2 are approached. Outside the range of rhythmicity, the system generates damped oscillations that eventually converge to an equilibrium value. At both ends of the temperature range, the breakdown of the clock occurs through a supercritical Hopf bifurcation in which the attractor of the system changes from a stable equilibrium point - representing an arrhythmic system - to a stable limit cycle - representing an autonomous oscillator. This can be seen in figure 7 below which shows the variation of the attractor with temperature. The loss of rhythmicity near the ends of the range was observed to be typical of solutions produced through local compensation at intermediate temperatures. Furthermore, the solutions retaining rhythmicity across the range had quadratic period-temperature profiles and so were unable to generate the monotonically decreasing (under-compensated) profiles reported in experiments [20], [8].

These results illustrate that the WT period-temperature and protein-temperature profiles observed experimentally can be qualitatively reproduced using isoform switching. In particular, the tuning of the difference Δp between the periods at the temperature extremes enables the controlled decrease in the WT experimental period profile to be easily simulated. In contrast, single-point

compensation is unable to simulate such a profile, illustrating the limitations of the technique as a viable mechanism for period control in realistic systems.

5 Simulating compensation mutants producing only one form of FRQ

Four mutant *Neurospora* strains in which one FRQ form is produced in abundance relative to the other were considered. Two of these were the splice site mutants I-6$^{\mathrm{opt}}$ and I-6$^{\mathrm{mut}}$ constructed by Diernfellner and coworkers [8]. In I-6$^{\mathrm{opt}}$ the splice sites of intron 6, which contains AUG #1, are optimised towards consensus. This gives rise to a strain in which s-FRQ is efficiently synthesised at all temperatures while l-FRQ is produced at low levels. In I-6$^{\mathrm{mut}}$, the splice sites are mutagenised towards nonsplice sites, leading to a strain in which l-FRQ is synthesised across the temperature range, and only trace amounts of s-FRQ are detectable [8]. I-6$^{\mathrm{opt}}$ and I-6$^{\mathrm{mut}}$ are referred to here and in the main paper as strains A and B respectively.

The other two mutant strains modelled were the AUG deletion constructs YL34 and JC101 of Liu and coworkers [20]. YL34 - obtained by deletion of AUG #1 - produces mainly s-FRQ while JC101 - obtained by point mutation of AUG #3 - produces mainly l-FRQ [20]. Here, YL34 and JC101 are referred to as strains C and D respectively.

5.1 Modelling of strains producing mainly s-FRQ

Strain A was modelled using s-FRQ and l-FRQ translation rate-temperature profiles $r_S(T)$ and $r_L(T)$ in which r_S increases with T and r_L is small compared to r_S across the temperature range. To model strain C, profiles were chosen in which r_L is at low levels, reflecting the deletion of AUG #1, and r_S decreases as T is increased, modelling the shift to AUG #1 due to thermosensitive splicing [2].

5.2 Modelling of strains producing mainly l-FRQ

To model strain B, translation profiles were used in which r_L increases with T and r_S is small compared to r_L. Strain D was modelled with profiles in which r_S was at low levels across the temperature range, reflecting the deletion of AUG #3, and r_L increases significantly with increasing temperature, modelling the combined effects of the shift to AUG #1 due to thermosensitive splicing and the increase in the size of the overall FRQ pool resulting from enhanced ribosome scanning efficiency [2].

For all modelled strains, the magnitudes of r_S and r_L were bounded so that the net translation rate $r_T = r_S + r_L$ was of similar order to the wild-type.

5.3 Results

Plots of the translation profiles $r_S(T)$ and $r_L(T)$ employed to model strains A-D for model 1 can be seen in figure 2. Figure 2 of the main paper shows the profiles used for model 2. The corresponding tanh function parameters determining the profiles through equations (14) and (15) are given in tables 4 and 9. Figure 4 shows the period-temperature relationships simulated using these profiles for model 1. The corresponding plots for model 2 are presented in figure 3 of the main paper.

Simulations of strains C and D

For both models, the simulated l-FRQ deletion construct YL34 (strain C) is compensated at low temperatures with a significantly increased period compared to the wild-type, becoming arrhythmic at the upper end of the temperature range. The simulated s-FRQ deletion construct JC101 (strain D) is compensated at high temperatures with a smaller period than that of the wild-type, becoming arrhythmic at the lower end of the temperature range. These simulations agree with the experimental results of Liu et al [20].

Simulations of strains A and B

For the simulated mutagenised splice-site mutant I-6$^{\mathrm{mut}}$ (strain B), modification of translation only gave a monotonic decrease in period, in agreement with experimental data [8], [7]. A decreasing period profile was also observed for the optimised splice-site mutant I-6$^{\mathrm{opt}}$ of Diernfellner et al (strain A), inconsistent with the increase in period observed experimentally [8], [7]. The decreasing profiles obtained for A and B are a consequence of the fact that, by construction, the wild-type solutions are roughly close to being symmetric in the FRQ loops. Consequently, the models can be approximated by reduced models involving only the net FRQ translation rate $r_F = r_S + r_L$ (recall the construction of the starting parameter sets for isoform switching in section 3). Rewriting the wild-type parameters in the reduced models as $\mathbf{k} = (k_1, \ldots, k_{m'-1}, r_F)$ implies the following expression for $\frac{dp}{dT}$ (cf. equation (19)):

$$\frac{dp}{dT}(\mathbf{k}) = \frac{1}{RT^2} \sum_{j=1}^{m'-1} \frac{\partial p}{\partial k_j}(\mathbf{k})\, k_j E_j + \frac{\partial p}{\partial r_F}(\mathbf{k})\, r'_F. \tag{26}$$

The parameters for the simulations of strains A and B can be written as $\bar{\mathbf{k}} = (k_1, \ldots, k_{m'-1}, \bar{r}_F)$ where $\bar{r}_F(T) = r_F(T) + \delta r_F(T)$ is the change in net FRQ translation resulting from replacing $r_S(T)$ with $\bar{r}_S(T) = r_S(T) + \delta r_S(T)$ and $r_L(T)$ with $\bar{r}_L(T) = r_L(T) + \delta r_L(T)$. Substituting $\bar{\mathbf{k}}$ into (26) and using Taylor expansions leads to the approximation below:

$$\begin{aligned}\frac{dp}{dT}\left(\bar{\mathbf{k}}\right) \approx \frac{dp}{dT}(\mathbf{k}) &+ \left(\frac{1}{RT^2} \sum_{j=1}^{m'-1} \frac{\partial^2 p}{\partial r_F \partial k_j}(\mathbf{k})\, k_j E_j + \frac{\partial^2 p}{\partial r_F^2}(\mathbf{k})\, r'_F \right) \delta r_F \\ &+ \left(\frac{\partial p}{\partial r_F}(\mathbf{k}) + \frac{\partial^2 p}{\partial r_F^2}(\mathbf{k})\, \delta r_F \right) \delta r'_F. \end{aligned} \tag{27}$$

In the simulations of all mutant strains, the FRQ translation profiles were bounded so that the net translation profile $\bar{r}_F$ was comparable to the wild-type; both δr_F and $\delta r'_F$ are therefore small compared to r_F. It follows from (27) that $\frac{dp}{dT}\left(\bar{\mathbf{k}}\right)$ will be of the same sign as $\frac{dp}{dT}(\mathbf{k})$ across (T_1, T_2), resulting in simulations of strains A and B in which period decreases with temperature, as in the wild-type.

If it is assumed, however, that there is a significant difference between the parameters in the s-FRQ and l-FRQ loops, simulations of strain A can be obtained for which period increases above the wild-type value with temperature, in agreement with the experiments reported in [8] and [7]. This can be seen by considering the expressions for $\frac{dp}{dT}$ in the wild-type and mutant at the upper end of the temperature range. Writing the WT parameters as $\mathbf{k} = (k_1, \ldots, k_{m-2}, r_S, r_L)$ and using the fact the l-FRQ loop dominates the s-FRQ loop at higher temperatures for the WT gives the

following approximation:

$$\frac{dp}{dT}(\mathbf{k}) \approx \frac{1}{RT^2}\sum_{j\in N}\frac{\partial p}{\partial k_j}(\mathbf{k})\,k_jE_j + \frac{1}{RT^2}\sum_{j\in L_L\setminus r_L}\frac{\partial p}{\partial k_j}(\mathbf{k})\,k_jE_j + \frac{\partial p}{\partial r_L}(\mathbf{k})\,r'_L. \tag{28}$$

Expressing the strain A parameters as $\bar{\mathbf{k}} = (k_1, \ldots, k_{s-2}, \bar{r}_S, \bar{r}_L)$, where $\bar{r}_S$ and $\bar{r}_L$ are defined as in the symmetric case, and using the domination of the s-FRQ loop over the l-FRQ loop in the mutant at higher temperatures yields:

$$\frac{dp}{dT}(\bar{\mathbf{k}}) \approx \frac{1}{RT^2}\sum_{j\in N}\frac{\partial p}{\partial k_j}(\bar{\mathbf{k}})\,k_jE_j + \frac{1}{RT^2}\sum_{j\in L_S\setminus r_S}\frac{\partial p}{\partial k_j}(\bar{\mathbf{k}})\,k_jE_j + \frac{\partial p}{\partial r_S}(\bar{\mathbf{k}})\,r'_S.$$

Taylor expanding the derivatives in the expression above and using (28) leads to the following:

$$\begin{aligned}\frac{dp}{dT}(\bar{\mathbf{k}}) \approx \frac{dp}{dT}(\mathbf{k}) &+ \frac{1}{RT^2}\left(\sum_{j\in L_S\setminus r_S}\frac{\partial p}{\partial k_j}(\mathbf{k})\,k_jE_j - \sum_{j\in L_L\setminus r_L}\frac{\partial p}{\partial k_j}(\mathbf{k})\,k_jE_j\right) + \frac{\partial p}{\partial r_S}(\mathbf{k})\,r'_S - \frac{\partial p}{\partial r_L}(\mathbf{k})\,r'_L \\ &+ \left(\frac{1}{RT^2}\sum_{j\in N\cup(L_S\setminus r_S)}\frac{\partial^2 p}{\partial r_L\partial k_j}(\mathbf{k})\,k_jE_j + \frac{\partial^2 p}{\partial r_L\partial r_S}(\mathbf{k})\,r'_S\right)\delta r_L + \left(\frac{\partial p}{\partial r_S}(\mathbf{k}) + \frac{\partial^2 p}{\partial r_L\partial r_S}(\mathbf{k})\,\delta r_L\right)\delta r'_S.\end{aligned}$$

The lower order terms in this approximation to $\frac{dp}{dT}(\bar{\mathbf{k}})$ show that it is possible to make $\frac{dp}{dT}(\bar{\mathbf{k}})$ positive - even though $\frac{dp}{dT}(\mathbf{k})$ is negative - by tuning the difference between the s-FRQ and l-FRQ loops appropriately. In the resulting simulation of strain A, period will increase with temperature at the upper end of the range. Consequently, if the FRQ translation profiles are such that $p(T_1) < p(T_2)$ and $\frac{dp}{dT}(\bar{\mathbf{k}})$ does not vary too much over (T_1, T_2), period will increase with temperature across all of (T_1, T_2).

Parameter values, activation energies and period derivatives at T_1 and T_2 for FRQ loop parameters that give increasing period profiles for strain A in the models are listed in tables 5 and 10. The tanh function parameters determining the corresponding FRQ translation profiles can be seen in tables 4 and 9.

6 Quantifying the relationship between FRQ level and rhythmicity

A number of experiments have suggested a link between FRQ protein levels and robust free-running rhythmicity of the *Neurospora* clock. In particular, these experiments have lead to the hypothesis that a threshold level of FRQ is required for the clock to retain rhythmicity, and that this threshold level increases with temperature [20], [8].

The relationship between FRQ level and functionality was investigated by quantifying how the level of net FRQ translation rate $r_F = r_S + r_L$ at which the basic, near-symmetric *Neurospora* models switch between rhythmic and arrhythmic solutions varies with temperature. This was done by defining one-parameter families of models interpolating between the simulations of the deletion constructs of Liu et al. and the splice-site mutants of Diernfellner et al. At the lower end of the temperature range, families of models interpolating between strains D (arrhythmic) and B (rhythmic) were obtained by writing the s-FRQ and l-FRQ translation rates r_S and r_L in the forms below:

$$r_S(T) = (1-\lambda)\,r_S^D(T) + \lambda r_S^B(T) \tag{29}$$

$$r_L(T) = (1-\lambda)\,r_L^D(T) + \lambda r_L^B(T). \tag{30}$$

Here, $\left\{r_S^D, r_L^D\right\}$ and $\left\{r_S^B, r_L^B\right\}$ represent the translation rates of strains D and B respectively, with λ an interpolation parameter. As λ varies between 0 and 1 for a given T, the model defined by (29)-(30) varies between the corresponding simulations of strains D and B. $r_F(T)$ therefore changes from a value for which the system is arrhythmic at T to a value for which it is rhythmic; the intermediate value at which the transition from an arrhythmic to a rhythmic state occurs, $r_F^L(T)$, represents the threshold net FRQ translation rate required for the system to oscillate. Dynamically, the transition takes place through a supercritical Hopf bifurcation, the same mechanism by which the locally compensated solution discussed in section 4.5.2 loses rhythmicity at the ends of the range. By using standard linear stability analysis to calculate the values of λ at which the Hopf bifurcation occurs, $r_F^L(T)$ could be determined over the lower temperature range.

At the upper end of the temperature range, families of models interpolating between strains C (arrhythmic) and A (rhythmic) were obtained by writing r_S and r_L as

$$r_S(T) = (1-\lambda) r_S^C(T) + \lambda r_S^A(T) \quad (31)$$

$$r_L(T) = (1-\lambda) r_L^C(T) + \lambda r_L^A(T), \quad (32)$$

where $\left\{r_S^C, r_L^C\right\}$ and $\left\{r_S^A, r_L^A\right\}$ represent the translation rates of strains C and A. At a given T, varying λ between 0 and 1 switches the model defined by (31)-(32) between the corresponding simulations of strains C and A. This enabled $r_F^L(T)$ to be determined across the high temperature range by calculating the corresponding Hopf bifurcation values of λ. $r_F^L(T)$ was determined at intermediate temperatures (where both strains C and D are rhythmic) by considering negative values of λ.

6.1 Verification of an increasing lower threshold for rhythmicity

Figure 4 of the main paper shows the variation of r_F^L with T for the second *Neurospora* model, computed using the method described above. These are the two solid curves close to the bottom of the picture (the leftmost curve represents the computation of $r_F^L(T)$ using (29)-(30) and the other curve the computation of $r_F^L(T)$ using (31)-(32)). It can be seen from the figure that r_F^L is an increasing function of T; that is the threshold level of FRQ translation required for a functional clock increases with temperature, as predicted experimentally [20]. The figures also shows that for the wild-type and strains A and B, the net translation rate r_F remains above r_F^L across (T_1, T_2). By contrast, r_F decreases below r_F^L near T_2 in strain C and decreases below r_F^L near T_1 in strain D. Thus, the loss of rhythmicity of the simulated AUG deletion constructs at the extremes of the temperature range is a result of sub-threshold levels of FRQ, in accordance again with experimental predictions [20], [8]. The insets to the figure illustrate the loss of rhythmicity through Hopf bifurcations (cf. figure 7 below). Outside the rhythmic ranges, strains C and D generate oscillations that damp to a constitutive level, in agreement with experiments (cf. figure 2 of [20]).

6.2 Prediction of an upper threshold for rhythmicity

In addition to quantifying the existence of an increasing minimum translation threshold for sustained oscillations, the models predict the existence of a temperature-dependent upper limit at which rhythmicity is lost as a consequence of excessive FRQ translation. This effect can be inferred from the form of the *frq* transcription equations (1) and (6) in the models. In both equations, high levels of FRQ can inhibit transcription sufficiently for the degradation term to dominate, causing

frq mRNA, M_F, to converge to a constitutive value, thereby stopping the clock. It follows that for a given temperature T, there is a net translation level $r_F^U(T)$ above which the system is arrhythmic.

The variation of this upper translation limit with temperature was determined by calculating the values of λ at which rhythmicity was lost as λ was increased from 1 in the models defined by (29)-(30) and (31)-(32). As in the case of subthreshold FRQ translation, the breakdown of the clock occurs through a Hopf bifurcation. The two solid curves at the top of figure 4 in the main paper represent the values of $r_F^U(T)$ calculated in this manner for model 2, with the leftmost and rightmost curves representing the values computed using (29)-(30) and (31)-(32) respectively. It is interesting to note that the net translation-temperature profiles of the simulated rhythmic *Neurospora* species lie reasonably close to the upper translation limits. This suggests that obtaining a functional clock is not simply a matter of perturbing the system so as to increase overall FRQ production; it requires appropriate tuning of the s- and l-FRQ translation profiles.

7 Variation of entrainment phase with temperature

Experiments have shown that, like many circadian species, *Neurospora* exhibits systematic variations in the phase of entrainment with photoperiod length [33], [24]. Such behaviour is consistent with the mathematical theory of coupled oscillators [11], [26]. This states that for a given forcing amplitude θ_M, as the difference $p - L$ between the period p of the free-running oscillator and the period L of the light-dark (LD) cycle increases through 0, the system switches from a quasiperiodic state to one where it is synchronised with the LD cycle before becoming quasiperiodic again. The region in $(p - L, \theta_M)$ space where the clock is synchronised is the Arnold tongue of the system. As p (or equivalently photoperiod length) is varied within the tongue for a given forcing strength, the phase of entrainment ϕ varies between 0 and 2π [26].

From the point of view of coupled oscillator theory, global compensation can be viewed in broadest terms as a process which ensures that at each temperature T within the physiological range, the period $p(T)$ of the clock is sufficiently close to 24h for the system to lie within the Arnold tongue [28]. It has been recently suggested that in *Neurospora*, $p(T)$ may also be specifically tuned so as to decrease with increasing T, thereby actively contributing to the buffering of entrainment phase against variations in temperature [8], [7]. Figure 8 shows period-temperature and phase-temperature profiles for simulations of the WT and strains A and B generated using model 2. These appear to support the buffering hypothesis: while phase remains relatively independent of temperature in the WT, there are significant changes in phase for the mutant strains.

In terms of mechanisms for period tuning, isoform switching enables a decreasing (or increasing) period profile to be easily obtained through adjustment of the difference in periods at the ends of the range, $\Delta p = p(T_2) - p(T_1)$ (cf. section 4.3). By contrast, since single-point compensation leads to a quadratic variation of period, it does not allow such adjustment of $p(T)$.

8 Robustness of the isoform switching mechanism

8.1 Switching through simulated annealing

The results reported above have shown that globally compensated systems representative of those reported experimentally can be obtained by directly applying isoform switching in the manner

described in section 4.4. In order to demonstrate the robustness of the mechanism - and indicate how it could arise through biological evolution - compensated systems were obtained from non-compensated ones using simulated annealing. In addition, the greater flexibility conferred by isoform switching was demonstrated by contrasting the evolved period profiles generated by models incorporating both s- and l-FRQ pathways (double-loop models) with models containing only one form of FRQ (single-loop models).

The annealing algorithm used was adapted from the optimisation technique described in section 3. For the single-loop models, the quantities varied were the activation energies E_k; for the double-loop models, the parameters $\{a_i, b_i, T_{S_i}, c_i\}$ determining the s- and l-FRQ translation profiles $r_S(T)$ and $r_L(T)$ were also varied in addition to the E_ks. The corresponding cost functions $C(E_k)/C(E_k, a_i, b_i, T_{S_i}, c_i)$ measured how close the system was at each annealing step to one with a constant period of 22.5h across the temperature range. 10000 annealing steps were used in each simulation with the starting annealing temperature set equal to the initial cost value.

8.2 Results

Figure 9 shows a representative simulation of global compensation generated through annealed isoform switching for model 1. The starting system in this case was obtained through random perturbations of the activation energies and FRQ translation profiles of the directly balanced solution derived in section 4.4. As can be seen in panel A of the figure, the starting system is non-compensated, losing functionality at lower temperatures. By contrast, the annealed system is functional over the whole range, with a near constant period-temperature relationship close to the target profile of the cost function. The activation energies and FRQ translation profiles of the annealed solution are significantly different from those of the directly balanced system, indicating that the annealing algorithm has converged to a compensated system distinct from the original one (see panels B and C of figure 9).

Figure 5 of the main paper compares typical annealed solutions generated from single- and double-loop systems for model 2. The starting point in both simulations was the symmetric system obtained by local compensation at the midpoint temperature T_C described in section 4.5.2; this system is compensated at intermediate temperatures but is non-functional at the ends of the range. The profiles shown are those obtained by annealing both single- and double-loop systems equivalent to the starting system.[4] The figure shows that for the double-loop model, annealing again recovers functionality, while also yielding a system with a period profile very close to the target zero-slope compensation of the cost function. By contrast the single-loop model does not fully recover functionality, becoming arrhythmic at the higher end of the temperature range, and is unable to generate a zero-slope profile.

These results demonstrate both the robustness and flexibility of the switching mechanism; randomised parameter changes readily tuned the noncompensated systems onto the codimension 3 surface of compensated ones. Furthermore, the annealing procedure tuned the double-loop systems so as to give specified period-temperature profiles, implying that such tuning could be obtained through evolutionary processes. The inability of the single-loop systems to match this degree of

[4]The equivalent single-loop system was generated by setting all parameters in the FRQ pathway equal to their corresponding values in the s-/l-FRQ loops, with the exception of FRQ translation which was set to the sum of the s- and l-FRQ rates. The equivalent double-loop system was derived by finding s- and l-FRQ translation profiles yielding a net translation profile equal to that of the symmetric one, while keeping the remaining parameters in the loops equal.

control suggests that the ability to tune the period profile through the variation of only 3 parameters conferred by isoform switching increases the evolutionary flexibility of the network.

9 Simulating compensation mutants resulting from changes in FRQ stability

Experiments and theoretical analysis have identified a link between the loss rate r of bulk FRQ protein and temperature compensation, with significant differences observed in r between wild-type strains and a number of mutant strains in which compensation is affected [30]. In simple models, such as the Goodwin oscillator used in [30], r is simply the degradation rate of FRQ transcription factor. In more complex models, such as those considered here, r will depend on parameters determining the transport, modification and degradation of all species involved in the conversion of FRQ into a transcription factor. Expressions are given below for the rates r and r' of s- and l-FRQ loss in the models. These are seen to depend on parameters with significant period derivatives, thereby confirming the dependence of the period-temperature profile on FRQ loss rate proposed in [30]. Furthermore, consideration of the control coefficients of these parameters in simulations of the FRQ stability mutants frq^1, frq^7 and frq^{S1531} identifies the critical parameters that may be affected in these strains.

9.1 The form of the overall FRQ loss rate in models 1 and 2

Following [30], r and r' can be calculated by considering the exponential decay of the FRQ forms from their LL equilibrium levels following a transfer to DD. It is fairly straightforward to show that for model 1:

$$\begin{aligned} r &= \frac{v_d k_2}{k_1 + k_2} \\ r' &= \frac{v'_d k'_2}{k'_1 + k'_2}, \end{aligned}$$

and for model 2:

$$r = \frac{d_2\left(f_1 + \gamma_1\left(2 + \frac{\gamma_1}{f_1}\right)\right)}{f_1 + d_2\left(2 + \frac{\gamma_1}{f_1}\right)} \tag{33}$$

$$r' = \frac{d'_2\left(f'_1 + \gamma'_1\left(2 + \frac{\gamma'_1}{f'_1}\right)\right)}{f'_1 + d'_2\left(2 + \frac{\gamma'_1}{f'_1}\right)}. \tag{34}$$

For both models, the loss rates involve one or more of the parameters with significant period derivatives identified earlier in section 4.5.1 (see tables 2 and 7). In particular, since f_1 and f'_1 are small, the FRQ loss rates for model 2 will depend significantly on the mean delay times $\tau = \frac{2}{f_1}$ and $\tau' = \frac{2}{f'_1}$ for just-translated s- and l-FRQ to become transcription factors.

9.2 Modelling the mutants by varying the loss rate

Figure 6 of the main paper plots simulations of the frq^1, frq^7 and frq^{S1531} period-temperature profiles $p(T)$ obtained by modifying the parameters contributing to the net FRQ loss rates r and r' for model 2. All the profiles are in qualitative agreement with experimental data [30].

Table 11 shows the FRQ pathway parameters used to generate the simulations, together with the corresponding values of r and r' computed using (33) and (34). For the simulated short-period frq^1 mutant, r and r' are seen to be greater than in the wild-type, indicating a decrease in the stability of the FRQ forms. By contrast, r and r' are smaller than the WT for the long-period frq^7 and frq^{S1531} strains, consistent with an increased stability of FRQ. Moreover, the loss rates are smaller for the simulated frq^{S1531} mutant than for the frq^7 mutant. These results are in qualitative agreement with experimental estimates of net FRQ loss for the strains [30]. Furthermore, the magnitudes of the control coefficients C_j^p for the parameters determining r and r' imply that the critical parameters affected in the strains are f_1 and f_1', controlling the mean times for s- and l-FRQ to become active transcription factors (i.e. the overall delays in the FRQ feedback loops); the parameters affecting the degradation of FRQ $\{d_2,d_2',\gamma_1,\gamma_1'\}$ have significantly smaller C_j^p values. f_1 and f_1' are reduced in frq^7 and frq^{S1531}, leading to a lengthening of period, while in frq^1, f_1 and f_1' are greater than their WT values, resulting in a shorter period phenotype. For the simulated frq^{S1531} mutant, the reduction in f_1 and f_1' can be interpreted as decreases in the FRQ phosphorylation rates. This is consistent with the fact that the mutant was obtained experimentally by replacing the phosphorylation site serine 513 on the FRQ ORF by isoleucine [30].

References

[1] Bell-Pedersen D, Crosthwaite SK, Lakin-Thomas PL, Merrow M, Okland M (2001) The *Neurospora* circadian clock: Simple or complex? *Philos. Trans. R. Soc. Lond. B Biol. Sci.* **356**(1415): 1697–1709

[2] Brunner M, Diernfellner, A (2006) How temperature affects the circadian clock of *Neurospora crassa*. *Chronobiol. Int.* **23**(1-2): 81–90

[3] Collett MA, Garceau N, Dunlap JC, Loros JJ (2002) Light and clock expression of the *Neurospora* clock gene frequency is differentially driven by but dependent on WHITE-COLLAR-2. *Genetics* **160**(1): 149–58

[4] Colot HV, Loros JJ, Dunlap JC (2005) Temperature-modulated alternative splicing and promoter use in the circadian clock gene frequency. *Mol. Biol. Cell* **16**(12): 5563–5571

[5] Crosthwaite SK, Loros JJ, Dunlap JC (1995) Light-induced resetting of a circadian clock is mediated by a rapid increase in frequency transcript. *Cell* **81**(7): 1003–12

[6] Denault DL, Loros JJ, Dunlap JC (2001) WC-2 mediates WC1-FRQ interaction within the PAS protein-linked circadian feedback loop of *Neurospora*. *EMBO J.* **20**(1-2): 109–17

[7] Diernfellner A, Colot HV, Dintsis O, Loros JJ, Dunlap JC, Brunner M (2007) Long and short isoforms of *Neurospora* clock protein FRQ support temperature-compensated circadian rhythms. *FEBS Lett.* doi:10.1016/ j.febslet.2007.11.043

[8] Diernfellner AC, Schafmeier T, Merrow MW, Brunner M (2005) Molecular mechanism of temperature sensing by the circadian clock of *Neurospora crassa*. *Genes Dev.* **19**(17): 1968–73

[9] Froehlich AC, Liu Y, Loros JJ, Dunlap JC (2002) White collar-1, a circadian blue light photoreceptor, binding to the frequency promoter. *Science* **297**(5582): 815–9

[10] Froehlich AC, Loros JJ, Dunlap JC (2003) Rhythmic binding of a WHITE COLLAR-containing complex to the frequency promoter is inhibited by FREQUENCY. *Proc. Natl. Acad. Sci. USA* **100**(10): 5914–9

[11] Gonze D, Goldbeter A (2000) Entrainment versus chaos in a model for a circadian oscillator driven by light-dark cycles. *J. Stat. Phys.* **101**(1-2): 649–663

[12] Gonze D, Halloy J, Goldbeter A (2002) Biochemical clocks and molecular noise: theoretical study of robustness factors. *J. Chem. Phys.* **116**: 10997–11010

[13] Kirkpatrick S, Gelatt CD, Vecchi MP (1983) Optimization by simulated annealing. *Science* **220**: 671–680

[14] Kurosawa G, Iwasa Y (2005) Temperature compensation in circadian clock models. *J. Theor. Biol.* **233**(4): 453–468

[15] Kurosawa G, Mochizuki A, Iwasa Y (2002) Comparative study of circadian clock models, in search of processes promoting oscillation. *J. Theor. Biol.* **216**(2): 193–208

[16] Lee K, Loros JJ, Dunlap JC (2000) Interconnected feedback loops in the *Neurospora* circadian system. *Science* **289**(5476): 107–10,

[17] Leloup JC, Gonze D, Goldbeter A (1999) Limit cycle models for circadian rhythms based on transcriptional regulation in *Drosophila* and *Neurospora*. *J. Biol. Rhythms* **14**(6): 433–448

[18] Linden H, Macino G (1997) White collar 2, a partner in blue-light signal transduction, controlling expression of light-regulated genes in *Neurospora crassa*. *EMBO J.* **16**(1): 98–109

[19] Liu Y (2003) Molecular mechanisms of entrainment in the *Neurospora* circadian clock. *J. Biol. Rhythms* **18**(3): 195–205

[20] Liu Y, Garceau NY, Loros JJ, Dunlap JC (1997) Thermally regulated translational control of FRQ mediates aspects of temperature responses in the *Neurospora* circadian clock. *Cell* **89**(3): 477–86

[21] Locke JCW, Millar AJ, Turner MS (2005) Modelling genetic networks with noisy and varied experimental data: The circadian clock in *Arabidopsis thaliana*. *J. Theor. Biol.* **234**(3): 383–93

[22] Locke JCW, Southern MM, Kozma-Bognar L, Hibberd V, Brown PE, Turner MS, Millar AJ (2005) Extension of a genetic network model by iterative experimentation and mathematical analysis. *Mol. Syst. Biol.* **1**: 2005.0013

[23] MacDonald N (1989) *Biological Delay Systems: Linear Stability Theory.* Cambridge: Cambridge University Press

[24] Merrow M, Boesl C, Ricken J, Messerschmitt M, Goedel M, Roenneberg T (2006) Entrainment of the *Neurospora* circadian clock. *Chronobiol. Int.* **23**(1-2): 71–80

[25] Merrow M, Franchi L, Dragovic Z, Gorl M, Johnson J, Brunner M, Macino G, Roenneberg T (2001) Circadian regulation of the light input pathway in *Neurospora crassa*. *EMBO J.* **20**(3): 307–15

[26] Pikosvky A, Rosenblum M, Kurths J (2001) *Synchronisation. A Universal Concept in Nonlinar Sciences.* Cambridge: Cambridge University Press

[27] Rand DA, Shulgin BV, Salazar JD, Millar AJ (2004) Design principles underlying circadian clocks. *J. R. Soc. Interface* **1**: 119–130,

[28] Rand DA, Shulgin BV, Salazar JD, Millar AJ (2006) Uncovering the design principles of circadian clocks: mathematical analysis of flexibility and evolutionary goals. *J. Theor. Biol.* **238**(3): 616–635

[29] Ruoff P, Christensen MK, Wolf J, Heinrich R (2003) Temperature dependency and temperature compensation in a model of yeast glycolytic oscillations. *Biophys. Chem.* **106**(2): 179–92

[30] Ruoff P, Loros JJ, Dunlap JC (2005) The relationship between FRQ-protein stability and temperature compensation in the *Neurospora* circadian clock. *Proc. Natl. Acad. Sci. USA* **102**(49): 17681–6

[31] Ruoff P, Rensing L (1996) The temperature-compensated Goodwin model simulates many circadian clock properties. *J. Theor. Biol.* **179**: 275–285

[32] Shampine L, Reichelt M, Kierzenka J (2000) Solving boundary value problems for ordinary differential equations in MATLAB with bvp4c. *http://www.mathworks.com/bvp_tutorial.* pp 1–27

[33] Tan Y, Dragovic Z, Roenneberg T, Merrow M (2004) Entrainment dissociates transcription and translation of a circadian clock gene in *Neurospora*. *Curr. Biol.* **14**(5): 433–8

Figures

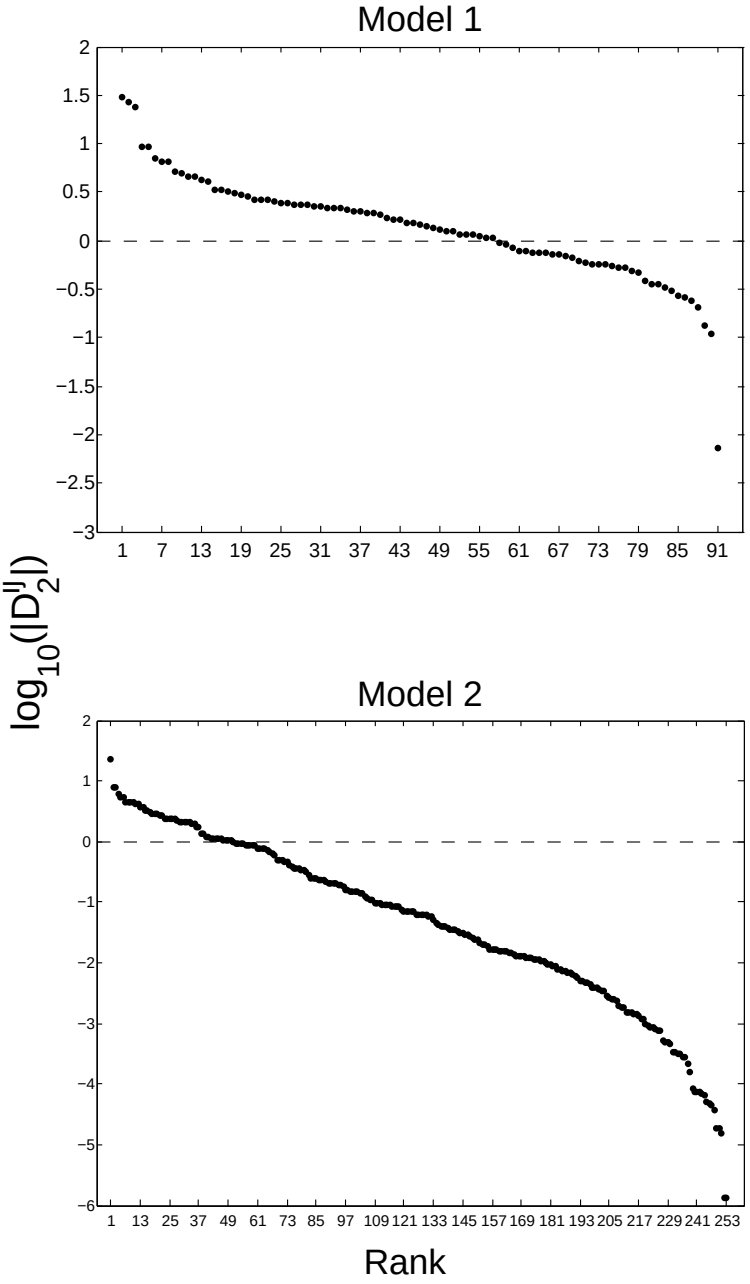

Figure 1: Magnitudes of the scaled second period derivatives $D_2^{ij} = k_i k_j \frac{\partial^2 p}{\partial k_i \partial k_j}$ for the two *Neurospora* models, ranked in order of size. The dotted lines indicate a derivative equal to 1. For both models, the derivatives were evaluated at the midpoint $T_C = 24$°C of the temperature range for parameter sets generating simulations of wild-type strains.

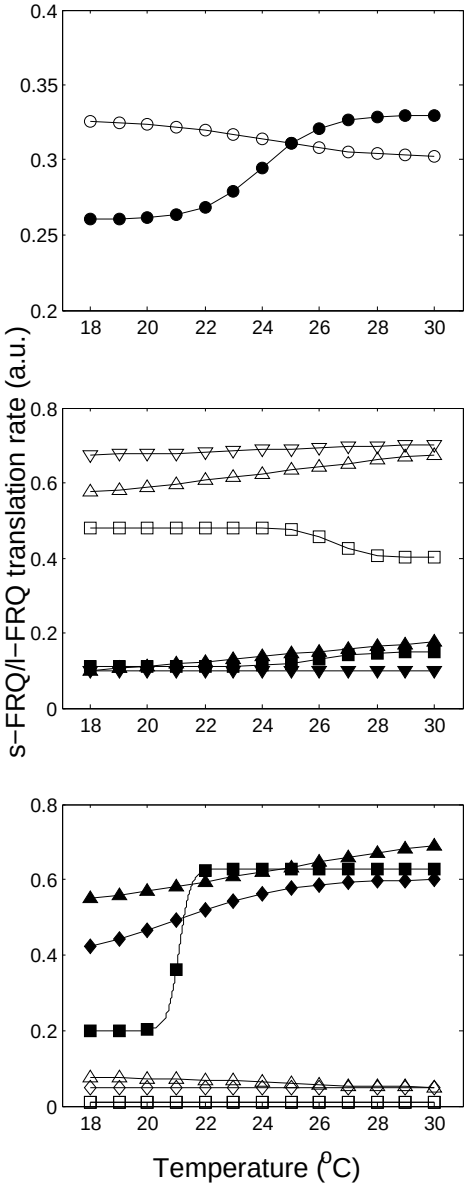

Figure 2: Variation of FRQ translation rates with temperature for the *Neurospora* strains simulated using model 1. Translation of s-FRQ and l-FRQ are denoted by open and closed symbols respectively. **Upper panel**. Wild-type. **Middle panel.** Strains producing mainly s-FRQ. Inverted triangles: strain A. Triangles: strain A with divergent FRQ pathways. Squares: strain C. **Lower panel**. Mutant strains producing mainly l-FRQ. Diamonds: strain B. Triangles: strain B with asymmetric FRQ pathways. Squares: strain D.

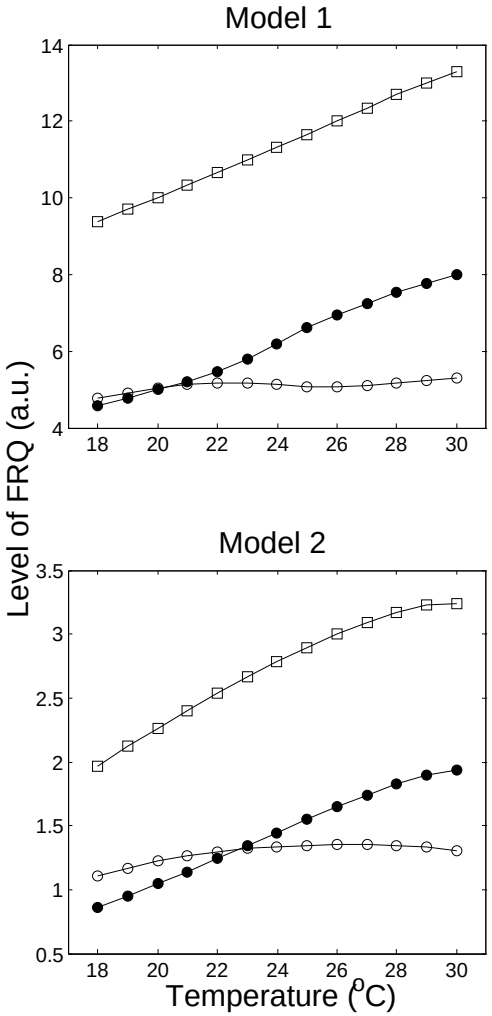

Figure 3: Variation with temperature of the levels of the FRQ isoforms for wild-type solutions simulated using the *Neurospora* models. Squares: total amount of FRQ. Filled circles: l-FRQ. Open circles: s-FRQ.

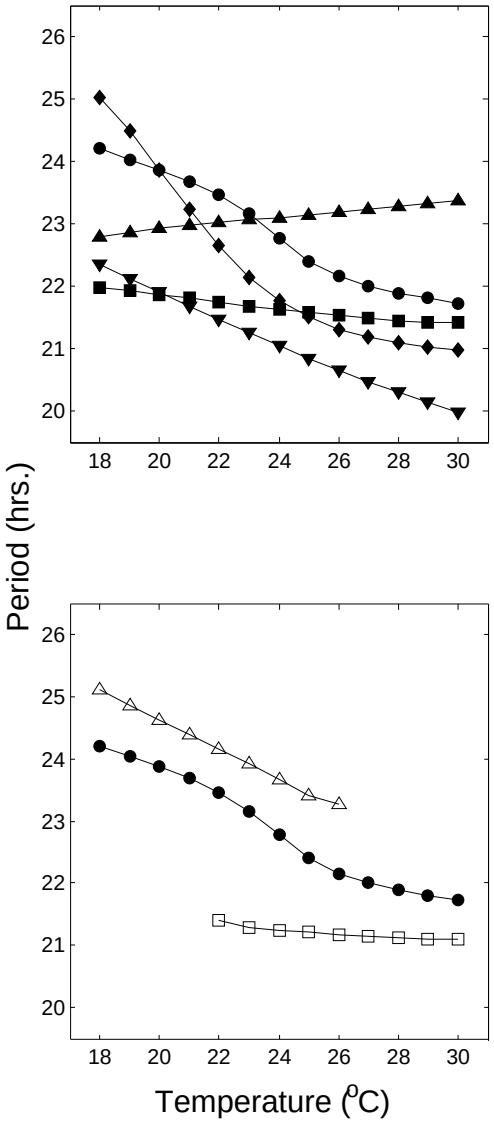

Figure 4: Period-temperature profiles simulated using model 1. Circles denote the simulation of the wild-type. **Upper panel.** Strains obtained through optimisation or suppression of thermosensitive splicing [8]. Inverted triangles: strain A. Triangles: strain A with asymmetric FRQ pathways. Diamonds: strain B. Squares: strain B with divergent FRQ pathways. **Lower panel.** Strains obtained through modification of the FRQ AUGs [20]. Triangles: strain C. Squares: strain D.

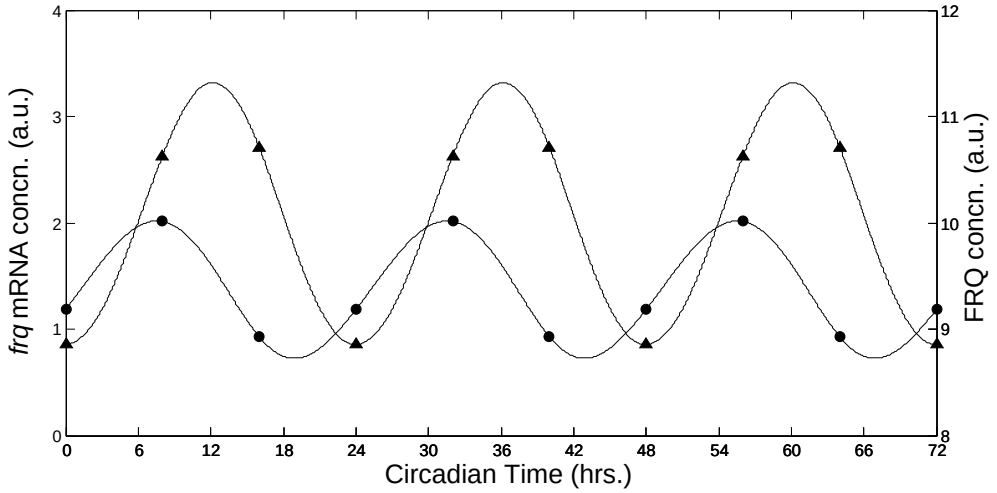

Figure 5: Time courses of *frq* mRNA (circles) and FRQ (triangles) simulated by model 1 at the midpoint $T_C = 24^{\circ}$C of the temperature range.

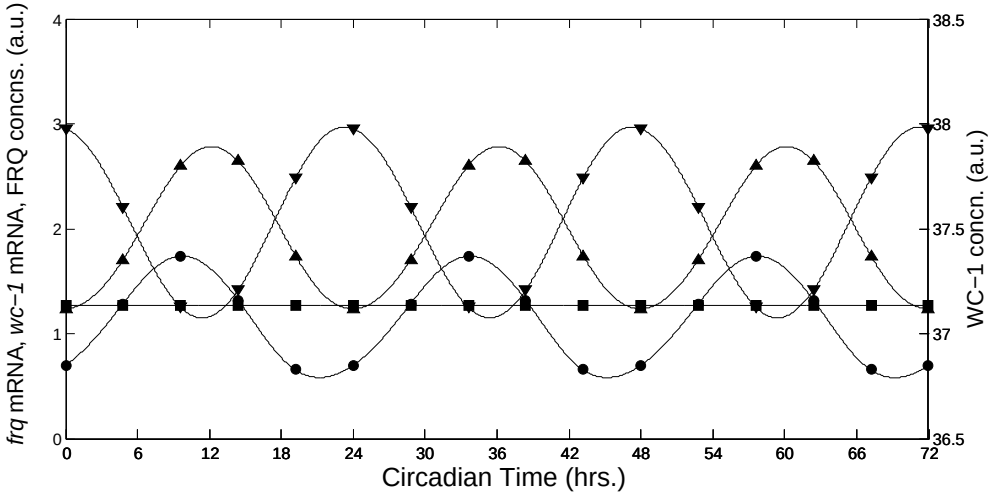

Figure 6: Time courses of *frq* mRNA (circles), FRQ (triangles), *wc-1* mRNA (squares) and WC-1 (inverted triangles) simulated by model 2 at the midpoint temperature $T_C = 24^{\circ}$C.

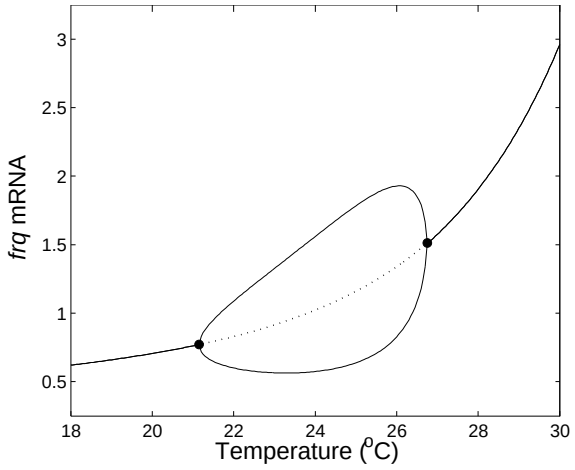

Figure 7: Bifurcation diagram illustrating the loss of rhythmicity in the system obtained through single-point compensation of model 2 at the centre of the temperature range $T_C = 24$°C. The values on the y-axis represent minimum and maximum levels of *frq* mRNA, with solid lines denoting stable attractors and dotted lines denoting unstable attractors. Solid circles indicate supercritical Hopf bifurcations where the attractor changes from a fixed point to a limit cycle.

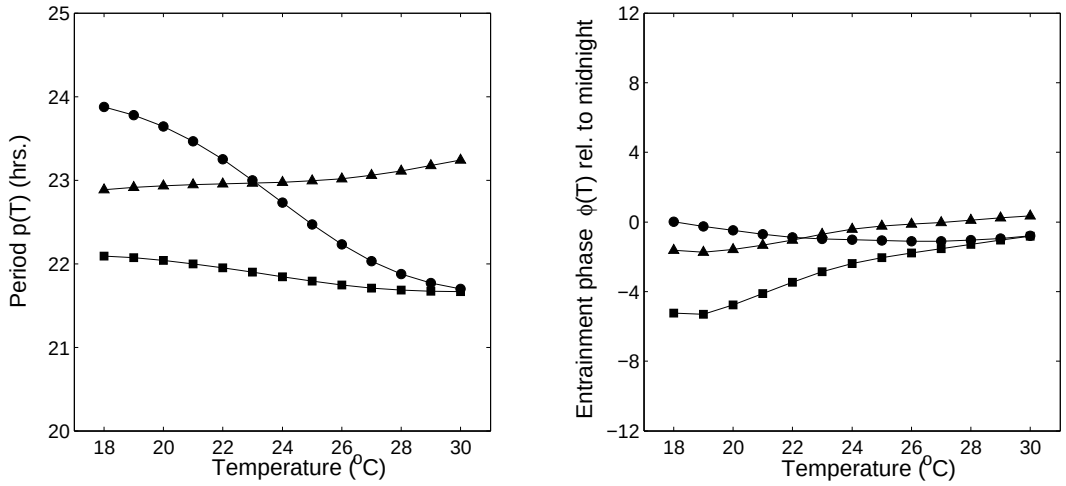

Figure 8: Period and entrainment phase profiles computed using model 2 (left and right panels respectively). Circles: wild-type. Triangles: strain A. Squares: strain B. Following [33], entrainment phase ϕ was taken to be the time at which FRQ reached its half-maximal value, computed relative to midnight. Photoperiod length was 12h.

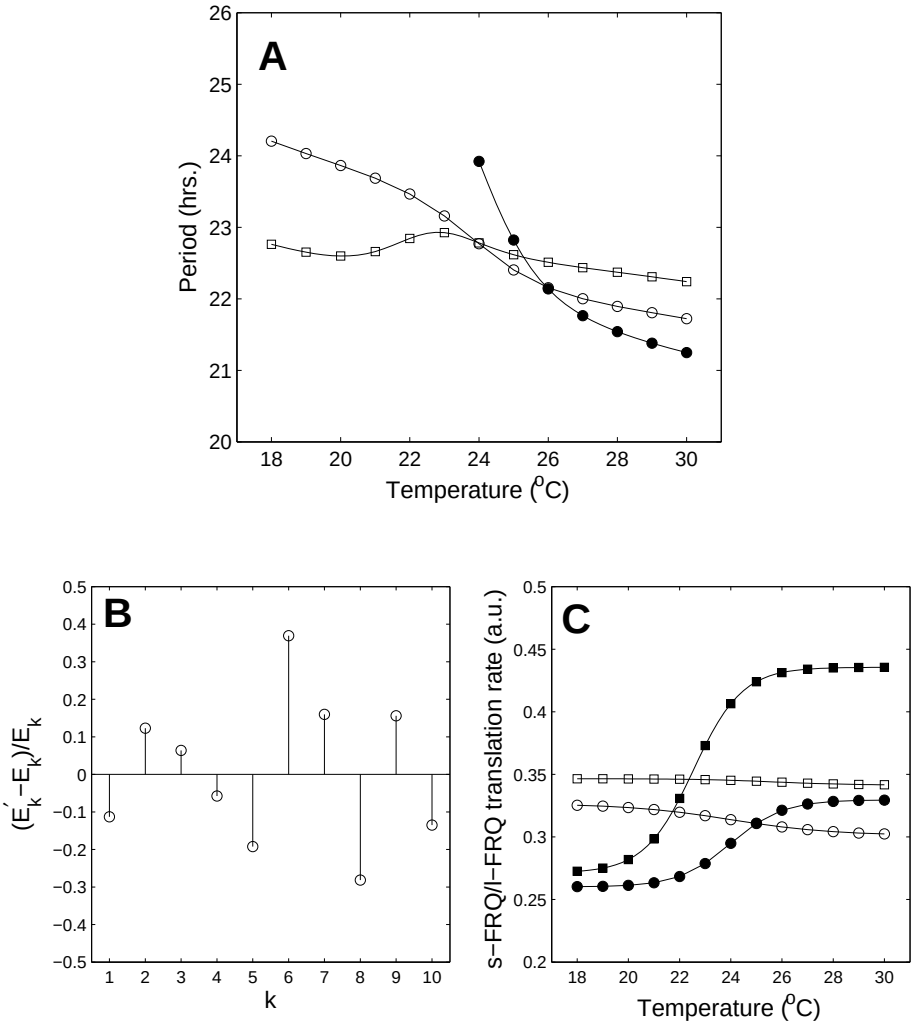

Figure 9: Global compensation of model 1 through isoform switching by simulated annealing. **Panel A.** Open circles: compensated solution generated through direct application of the switching method. Closed circles: noncompensated solution resulting from random perturbations of the FRQ translation profiles and the activation energies E_k affecting period; the system becomes arrhythmic as temperature is decreased. Squares: compensated system obtained by driving the non-compensated solution to a target period of 22.5h through simulated annealing. **Panel B.** Relative differences between the energies of the directly balanced system, E_k, and the annealed one, E'_k. **Panel C**. FRQ translation profiles of the directly balanced solution (circles) and the annealed solution (squares). Open and closed symbols denote translation of s- and l-FRQ respectively.

Tables

Table 1: Parameter values k_j, activation energies E_j, scaled period derivatives $k_j \frac{\partial p}{\partial k_j}$ and control coefficients C_j^p at the ends of the temperature range (T_1, T_2) for the wild-type solution simulated with model 1. The values of $\frac{dp}{dT}$ shown were computed using equation (20).

k_j	E_j, kJ mol^{-1}	$k_j\,(T_1)$	$k_j\,(T_2)$	$\left(k_j \frac{\partial p}{\partial k_j}\right)(T_1)$	$\left(k_j \frac{\partial p}{\partial k_j}\right)(T_2)$	$C_j^p\,(T_1)$	$C_j^p\,(T_2)$
Parameters outside the FRQ loops (N)							
v_s (h^{-1})	20.3717	1.0322	1.4408	-15.5044	-8.6265	-0.6406	-0.3971
K_I (nM)	33.3567	3.8189	6.5928	11.1738	9.3793	0.4616	0.4318
n	0	6.3958	6.3958	-6.1715	-6.0788	-0.2550	-0.2798
v_m (h^{-1})	12.9135	0.7949	0.9820	5.8399	0.3570	0.2413	0.0164
K_m (nM)	15.5174	0.0743	0.0958	-1.5092	-1.1096	-0.0624	-0.0511
s-FRQ loop parameters (L_S)							
k_s (h^{-1})	0	0.3253	0.3024	-5.3135	-4.2571	-0.2195	-0.1960
v_d (h^{-1})	13.3176	0.1442	0.1793	0.9221	0.2445	0.0381	0.0113
k_1 (h^{-1})	43.1253	0.1553	0.3146	-4.5296	-3.1405	-0.1871	-0.1446
k_2 (h^{-1})	21.3525	0.2774	0.3934	1.5945	1.0044	0.0659	0.0462
l-FRQ loop parameters. (L_L)							
k_s' (h^{-1})	0	0.2602	0.3294	-5.8602	-5.1221	-0.2421	-0.2358
v_d' (h^{-1})	4.3792	0.1347	0.1447	1.3200	0.7275	0.0545	0.0335
k_1' (h^{-1})	21.1308	0.2283	0.3226	-4.7434	-4.1251	-0.1960	-0.1899
k_2' (h^{-1})	2.9957	0.2881	0.3026	2.0705	1.2155	0.0855	0.0560
						$\frac{dp}{dT} = -0.1769$	$\frac{dp}{dT} = -0.0818$

Table 2: Reduced version of table 1 showing the temperature-dependent parameters for which $|C_j^p(T_1)| > 0.1$.

k_j	E_j, kJ mol^{-1}	$k_j\,(T_1)$	$k_j\,(T_2)$	$\left(k_j \frac{\partial p}{\partial k_j}\right)(T_1)$	$\left(k_j \frac{\partial p}{\partial k_j}\right)(T_2)$	$C_j^p\,(T_1)$	$C_j^p\,(T_2)$
Parameters outside the FRQ loops (N)							
v_s (h^{-1})	20.3717	1.0322	1.4408	-15.5044	-8.6265	-0.6406	-0.3971
K_I (nM)	33.3567	3.8189	6.5928	11.1738	9.3793	0.4616	0.4318
v_m (h^{-1})	12.9135	0.7949	0.9820	5.8399	0.3570	0.2413	0.0164
s-FRQ loop parameters (L_S)							
k_s (h^{-1})	0	0.3253	0.3024	-5.3135	-4.2571	-0.2195	-0.1960
k_1 (h^{-1})	43.1253	0.1553	0.3146	-4.5296	-3.1405	-0.1871	-0.1446
l-FRQ loop parameters. (L_L)							
k_s' (h^{-1})	0	0.2602	0.3294	-5.8602	-5.1221	-0.2421	-0.2358
k_1' (h^{-1})	21.1308	0.2283	0.3226	-4.7434	-4.1251	-0.1960	-0.1899

Table 3: Effect on the period Q_{10} of perturbing parameters with high control coefficients for the WT solution of model 1 about the midpoint temperature T_C. Values shown in brackets are the period changes at T_C. AR denotes a parameter change resulting in an arrhythmic system.

$k_j(T_C)$	$0.05k_j$	$0.25k_j$	$0.5k_j$	$0.9k_j$	$0.95k_j$	k_j	$1.05k_j$
Parameters outside the FRQ loops (N)							
v_s	AR	AR	AR	AR	1.12 (+0.7)	1.11	1.10 (-0.6)
K_I	AR	AR	1.09 (-6.1)	1.11 (-1.1)	1.11 (-0.5)	1.11	1.11 (+0.5)
v_m	AR	AR	1.07 (+3.4)	1.09 (-0.1)	1.10 (-0.1)	1.11	1.12 (+0.2)
s-FRQ loop parameters (L_S)							
k_s	AR	1.22 (+3.2)	1.17 (+2.0)	1.12 (+0.4)	1.11 (+0.2)	1.11	1.10 (-0.2)
k_1	AR	1.21 (+3.0)	1.17 (+1.8)	1.12 (+0.3)	1.11 (+0.2)	1.11	1.10 (-0.1)
l-FRQ loop parameters (L_L)							
k_s'	AR	AR	1.06 (+4.3)	1.10 (+0.7)	1.10 (+0.4)	1.11	1.11 (-0.3)
k_1'	AR	AR	1.06 (+3.8)	1.10 (+0.6)	1.11 (+0.3)	1.11	1.11 (-0.3)

Table 4: Parameters determining the translation-temperature profiles of the FRQ forms for model 1.

a_1	c_1	T_{S_1}	b_1	a_2	c_2	T_{S_2}	b_2
Wild-type							
-0.0127	0.3138	24.0000	0.2500	0.0348	0.2948	24.0000	0.5000
Strain A							
0.0138	0.6875	24.0000	0.2500	0	0.1000	-	-
Strain B							
0	0.0500	-	-	0.1085	0.4939	21.0000	0.2500
Strain C							
-0.0398	0.4402	26.5000	0.9000	0.0200	0.1300	26.0000	0.6500
Strain D							
0	0.0100	-	-	0.2138	0.4138	21.1000	2.5000
Wild-type: divergent FRQ loops							
-0.0070	0.2876	24.0000	0.2000	0.1698	0.3930	24.0000	0.1750
Strain A: divergent FRQ loops							
0.0931	0.6250	24.0000	0.1000	0.0698	0.1375	24.0000	0.1000
Strain B: divergent FRQ loops							
-0.0138	0.0625	24.0000	0.2500	0.1303	0.6200	24.0000	0.1000

Table 5: FRQ loop parameters for the WT system with divergent FRQ loops yielding an increasing strain A period profile for model 1.

k_j	E_j, kJ mol^{-1}	$k_j\,(T_1)$	$k_j\,(T_2)$	$\left(k_j\frac{\partial p}{\partial k_j}\right)(T_1)$	$\left(k_j\frac{\partial p}{\partial k_j}\right)(T_2)$	$C_j^p\,(T_1)$	$C_j^p\,(T_2)$
s-FRQ loop parameters (L_S)							
k_s $\left(\mathrm{h}^{-1}\right)$	0	0.2934	0.2817	-5.4485	-2.4428	-0.2251	-0.1124
v_d $\left(\mathrm{h}^{-1}\right)$	3.5176	0.1442	0.1527	1.2634	0.3025	0.0522	0.0139
k_1 $\left(\mathrm{h}^{-1}\right)$	1.2612	0.1582	0.1615	-4.6418	-2.0536	-0.1918	-0.0945
k_2 $\left(\mathrm{h}^{-1}\right)$	39.1957	0.2071	0.3934	1.5844	0.8826	0.0655	0.0406
l-FRQ loop parameters (L_L)							
k_s' $\left(\mathrm{h}^{-1}\right)$	0	0.2602	0.5257	-5.9289	-7.4766	-0.2450	-0.3441
v_d' $\left(\mathrm{h}^{-1}\right)$	4.3792	0.1347	0.1447	1.3599	1.5729	0.0562	0.0724
k_1' $\left(\mathrm{h}^{-1}\right)$	8.5615	0.2283	0.2626	-4.6302	-5.9650	-0.1913	-0.2746
k_2' $\left(\mathrm{h}^{-1}\right)$	2.9957	0.2881	0.3026	2.2327	2.4816	0.0922	0.1142

Table 6: Parameter values k_j, activation energies E_j, scaled period derivatives $k_j\frac{\partial p}{\partial k_j}$ and control coefficients C_j^p at the ends of the temperature range (T_1, T_2) for the wild-type solution simulated with model 2. $\frac{dp}{dT}$ was calculated using equation (20).

k_j	E_j, kJ mol^{-1}	$k_j\,(T_1)$	$k_j\,(T_2)$	$\left(k_j\frac{\partial p}{\partial k_j}\right)(T_1)$	$\left(k_j\frac{\partial p}{\partial k_j}\right)(T_2)$	$C_j^p\,(T_1)$	$C_j^p\,(T_2)$
Parameters outside the FRQ loops (N)							
a_1 $\left(\mathrm{h}^{-1}\right)$	117.4780	9.3639	64.0666	0	0	0	0
a_2 $\left(\mathrm{h}^{-1}\right)$	30.7765	2.7826	4.6052	9.0568	7.5701	0.3793	0.3489
a_4 $\left(\mathrm{h}^{-1}\right)$	50.2083	0.3040	0.6915	1.7931	0.2530	0.0751	0.0117
a_5 $\left(\mathrm{h}^{-1}\right)$	54.9713	0.0184	0.0453	0	0	0	0
a_6 $\left(\mathrm{h}^{-1}\right)$	16.4375	0.1804	0.2361	0.0255	0.0069	0.0011	0.0003
a_7 $\left(\mathrm{h}^{-1}\right)$	47.8978	2.0302	4.4469	0.0309	0.0251	0.0013	0.0012
b_1 $\left(\mathrm{nM}^{-1}\right)$	3.0921	0.0020	0.0021	0	0	0	0
b_2 (nM)	19.7912	1.8096	2.5019	0	0	0	0
b_3 $\left(\mathrm{nM}^{-1}\right)$	7.2490	0.0757	0.0852	7.2615	6.6301	0.3042	0.3055
b_4 (nM)	11.2656	0.4174	0.5020	-0.0400	-0.0208	-0.0017	-0.0010
b_5 (nM)	33.7686	0.0985	0.1712	-0.2600	-0.0811	-0.0109	-0.0037
b_6 (nM)	5.1777	2.8418	3.0932	0	0	0	0
b_7 (nM)	49.5354	0.0738	0.1661	0.0565	0.0320	0.0024	0.0015
b_8 (nM)	16.7162	70.5378	92.7385	0.0401	0.0209	0.0017	0.0010
b_9 (nM)	5.2257	89.0643	97.0183	0	0	0	0
d_1 $\left(\mathrm{h}^{-1}\right)$	12.7443	1.2906	1.5860	-16.0275	-14.0939	-0.6713	-0.6495
d_3 $\left(\mathrm{h}^{-1}\right)$	56.5082	0.3138	0.7915	-1.7931	-0.2530	-0.0751	-0.0117

Table 6 continued.

k_j	E_j, kJ mol^{-1}	$k_j\,(T_1)$	$k_j\,(T_2)$	$\left(k_j \frac{\partial p}{\partial k_j}\right)(T_1)$	$\left(k_j \frac{\partial p}{\partial k_j}\right)(T_2)$	$C_j^p\,(T_1)$	$C_j^p\,(T_2)$
Parameters outside the FRQ loops (N)							
d_4 (h^{-1})	9.5152	3.1093	3.6333	-0.0564	-0.0321	-0.0024	-0.0015
d_5 (h^{-1})	4.3290	0.3963	0.4254	0	0	0	0
f_2 (h^{-1})	20.9735	0.1257	0.1772	-0.0004	-0.0006	-1.5912e-5	-2.6024e-5
γ_2 (h^{-1})	31.3752	0.0002	0.0004	-0.0002	-0.0001	-7.9997e-6	-5.9409e-6
r_1 (h^{-1})	109.8902	1.0849	6.5556	0	0	0	0
r_2 (h^{-1})	3.0244	34.5172	36.2691	0	0	0	0
n	0	1.0242	1.0242	0	0	0	0
m	0	1.3498	1.3498	0.1696	0.0955	0.0071	0.0044
k	0	2.1823	2.1823	0	0	0	0
s-FRQ loop parameters (L_S)							
a_3 (h^{-1})	0	0.3175	0.2624	-3.8276	-3.2001	-0.1603	-0.1475
d_2 (h^{-1})	16.7070	0.1848	0.2430	0.0287	0.2730	0.0012	0.0126
f_1 (h^{-1})	24.8967	0.0815	0.1225	-7.2212	-5.7781	-0.3025	-0.2663
γ_1 (h^{-1})	8.8560	0.3561	0.4116	1.8964	2.0903	0.0794	0.0963
l-FRQ loop parameters (L_L)							
a_3' (h^{-1})	0	0.2479	0.3626	-3.4030	-3.4048	-0.1425	-0.1569
d_2' (h^{-1})	2.2653	0.1785	0.1852	0.0698	-0.1162	0.0029	-0.0054
f_1' (h^{-1})	9.8836	0.0883	0.1038	-6.3518	-6.4308	-0.2661	-0.2964
γ_1' (h^{-1})	1.8012	0.3703	0.3814	1.9053	1.3922	0.0798	0.0642
						$\frac{dp}{dT} = -0.1440$	$\frac{dp}{dT} = -0.0937$

Table 7: Reduced version of table 6 showing the temperature-dependent parameters for which $|C_j^p(T_1)| > 0.0775$.

k_j	E_j, kJ mol^{-1}	$k_j\,(T_1)$	$k_j\,(T_2)$	$\left(k_j \frac{\partial p}{\partial k_j}\right)(T_1)$	$\left(k_j \frac{\partial p}{\partial k_j}\right)(T_2)$	$C_j^p\,(T_1)$	$C_j^p\,(T_2)$
Parameters outside the FRQ loops (N)							
a_2 (h^{-1})	30.7765	2.7826	4.6052	9.0568	7.5701	0.3793	0.3489
b_3 (nM^{-1})	7.2490	0.0757	0.0852	7.2615	6.6301	0.3042	0.3055
d_1 (h^{-1})	12.7443	1.2906	1.5860	-16.0275	-14.0939	-0.6713	-0.6495
s-FRQ loop parameters (L_S)							
a_3 (h^{-1})	0	0.3175	0.2624	-3.8276	-3.2001	-0.1603	-0.1475
f_1 (h^{-1})	24.8967	0.0815	0.1225	-7.2212	-5.7781	-0.3025	-0.2663
γ_1 (h^{-1})	8.8560	0.3561	0.4116	1.8964	2.0903	0.0794	0.0963
l-FRQ loop parameters (L_L)							
a_3' (h^{-1})	0	0.2479	0.3626	-3.4030	-3.4048	-0.1425	-0.1569
f_1' (h^{-1})	9.8836	0.0883	0.1038	-6.3518	-6.4308	-0.2661	-0.2964
γ_1' (h^{-1})	1.8012	0.3703	0.3814	1.9053	1.3922	0.0798	0.0642

Table 8: Effect on the period Q_{10} of perturbing parameters with high control coefficients for the WT solution of model 2 about the midpoint temperature T_C. Values shown in brackets are the period changes at T_C. AR denotes a perturbation resulting in an arrhythmic system. (Note: the mean delay times for s- and l-FRQ transcription factor conversion are $\tau = \frac{2}{f_1}$ and $\tau' = \frac{2}{f_1'}$ respectively).

$k_j(T_C)$	$0.05k_j$	$0.25k_j$	$0.5k_j$	$0.9k_j$	$0.95k_j$	k_j	$1.05k_j$
Parameters outside the FRQ loops (N)							
a_2	AR	AR	AR	1.09 (-0.9)	1.09 (-0.4)	1.09	1.09 (+0.4)
b_3	AR	AR	AR	1.09 (-0.7)	1.09 (-0.4)	1.09	1.09 (+0.3)
d_1	AR	AR	AR	1.09 (+1.6)	1.09 (+0.8)	1.09	1.09 (-0.7)
s-FRQ loop parameters (L_S)							
a_3	1.17 (+4.7)	1.15 (+3.4)	1.12 (+2.0)	1.10 (+0.3)	1.09 (+0.2)	1.09	1.09 (-0.2)
f_1	1.21 (+5.0)	1.18 (+4.6)	1.15 (+3.3)	1.10 (+0.6)	1.10 (+0.3)	1.09	1.09 (-0.3)
γ_1	AR	AR	AR	1.10 (-0.1)	1.09 (-0.1)	1.09	1.09 (+0.1)
l-FRQ loop parameters (L_L)							
a_3'	0.95 (+5.4)	1.02 (+3.8)	1.06 (+2.2)	1.09 (+0.4)	1.09 (+0.2)	1.09	1.09 (-0.2)
f_1'	AR	AR	1.04 (+3.6)	1.08 (+0.7)	1.09 (+0.3)	1.09	1.10 (-0.3)
γ_1'	AR	AR	AR	1.09 (-0.2)	1.09 (-0.1)	1.09	1.09 (-0.1)

Table 9: Parameters determining the FRQ translation-temperature profiles for model 2.

a_1	c_1	T_{S_1}	b_1	a_2	c_2	T_{S_2}	b_2
Wild-type							
-0.0304	0.2900	24.0000	0.2500	0.0576	0.3053	24.0000	0.5000
Strain A							
0.0070	0.6650	24.0000	0.5000	0	0.0560	-	-
Strain B							
0	0.0140	-	-	0.1909	0.5553	21.0000	0.2500
Strain C							
-0.0384	0.4132	24.0000	0.2500	0	0.0140	-	-
Strain D							
0	0.0014	-	-	0.3195	0.4035	21.1500	2.5000
Wild-type: divergent FRQ loops							
0.0128	0.2964	24.0000	0.2500	0.1607	0.3588	25.0000	0.1750
Strain A: divergent FRQ loops							
0.0077	0.5670	24.0000	0.2500	0	0.0350	0	0
Strain B: divergent FRQ loops							
0.0077	0.0350	24.0000	0.2500	0.1299	0.6843	24.0000	0.1000

Table 10: FRQ loop parameters for the WT system with divergent loops yielding an increasing strain A period profile for model 2.

k_j	E_j, kJ mol^{-1}	$k_j\,(T_1)$	$k_j\,(T_2)$	$\left(k_j \frac{\partial p}{\partial k_j}\right)(T_1)$	$\left(k_j \frac{\partial p}{\partial k_j}\right)(T_2)$	$C_j^p\,(T_1)$	$C_j^p\,(T_2)$
s-FRQ loop parameters (L_S)							
a_3 (h^{-1})	0	0.2848	0.3080	-3.8825	-2.7132	-0.1626	-0.1250
d_2 (h^{-1})	16.7070	0.1848	0.2430	-0.0032	0.1521	-0.0001	0.0070
f_1 (h^{-1})	11.3784	0.0845	0.1018	-7.4827	-5.0176	-0.3134	-0.2312
γ_1 (h^{-1})	21.9415	0.2881	0.4126	0.9622	1.6569	0.0403	0.0764
l-FRQ loop parameters (L_L)							
a_3' (h^{-1})	0	0.2237	0.47195	-3.1640	-3.9723	-0.1325	-0.1831
d_2' (h^{-1})	2.2653	0.1785	0.1852	0.2080	-0.0516	0.0087	-0.0024
f_1' (h^{-1})	6.1204	0.0911	0.1007	-5.8637	-7.4108	-0.2456	-0.3415
γ_1' (h^{-1})	9.6287	0.3702	0.4334	1.8870	2.2978	0.0790	0.1059

Table 11: Parameter values k_j and control coefficients C_j^p of the FRQ loop pathways for model 2 yielding the simulations of the *frq*^{1}, *frq*^{7} and *frq*^{S1531} period-temperature profiles shown in figure 6 of the main paper. r and r' denote the net loss of s-FRQ and l-FRQ respectively, as calculated from equations (33) and (34).

	Wild-type				*frq*^{1}			
k_j	$k_j\,(T_1)$	$k_j\,(T_2)$	$C_j^p\,(T_1)$	$C_j^p\,(T_2)$	$k_j\,(T_1)$	$k_j\,(T_2)$	$C_j^p\,(T_1)$	$C_j^p\,(T_2)$
r	0.3450	0.3971	-	-	0.3885	0.4119	-	-
d_2	0.1848	0.2430	0.0012	0.0126	0.2552	0.2943	0.0062	0.0015
f_1	0.0815	0.1225	-0.3025	-0.2663	0.1317	0.1624	-0.2945	-0.2287
γ_1	0.3561	0.4116	0.0794	0.0963	0.4021	0.4259	0.0724	0.0527
r'	0.3561	0.3637	-	-	0.3697	0.3826	-	-
d_2'	0.1785	0.1852	0.0029	-0.0054	0.2645	0.3661	0.0053	0.0150
f_1'	0.0883	0.1038	-0.2661	-0.2964	0.1384	0.1594	-0.2574	-0.3159
γ_1'	0.3703	0.3814	0.0798	0.0642	0.3813	0.3842	0.0575	0.0650
	frq^7				*frq*^{S1531}			
k_j	$k_j\,(T_1)$	$k_j\,(T_2)$	$C_j^p\,(T_1)$	$C_j^p\,(T_2)$	$k_j\,(T_1)$	$k_j\,(T_2)$	$C_j^p\,(T_1)$	$C_j^p\,(T_2)$
r	0.1844	0.2039	-	-	0.1094	0.1656	-	-
d_2	0.1507	0.1716	0.0280	0.0380	0.1332	0.1598	0.0379	0.0470
f_1	0.0463	0.0836	-0.3644	-0.3219	0.0255	0.0599	-0.3136	-0.3308
γ_1	0.1861	0.2074	0.0453	0.0535	0.1087	0.1661	0.0606	0.0633
r	0.1476	0.1788	-	-	0.1299	0.1346	-	-
d_2'	0.1675	0.2124	0.0224	0.0280	0.1551	0.1932	0.0118	0.0535
f_1'	0.0413	0.0643	-0.2349	-0.2749	0.0289	0.0488	-0.3052	-0.3169
γ_1'	0.1467	0.1767	0.0305	0.0393	0.1292	0.1314	0.0195	0.0814